Universidad Michoacana de San Nicolás de Hidalgo

Instituto de Física y Matemáticas

Dark energy properties in light of cosmological observations.

Tesis presentada al
Instituto de Física y Matemáticas

como requisito parcial para la obtención del grado de
Doctora en Ciencias en el Área de Física.

Por

Gabriela García Arroyo

asesorada por

Dr. Jorge Luis Cervantes Cota, Dr. Ulises Nucamendi Gómez

Morelia, Michoacán, México.
Enero del 2021

Acknowledgments

Foremost, I would like to express my sincere gratitude to my advisors, Dr. Ulises Nucamendi Gómez and Dr. Jorge Cervantes Cota, for all their help, support, immense patience and knowledge. This thesis and related works wouldn't be possible without their guidance. I've learned a lot of invaluable things from them that I'm sure are going to help me in all the aspects of my future life.

I would like to express a special thank to Dr. Alejandro Avilés whose expertise and knowledge into the subject matter helped me through this research. Also I want to acknowledge to my committee members, Dr. Mario Alberto Rodriguez Meza, Dr. Francisco Astorga Saenz and Dr. Ricardo Becerril Bárcenas, for their opportune comments and suggestions.

I would like to acknowledge to the Instituto de Física y Matemáticas (IFM) of the Universidad Michoacana, whose installations were like a home from me during a part of my PhD study. I also thank to the Instituto Nacional de Investigaciones Nucleares (ININ) for the facilities and the opportunity to do an important part of my research in its installations.

The realization of this work wouldn't be possible without the financial support provided by the grant No. 290778 of Conacyt. Also thanks for the additional support from Conacyt project 283151.

Last but not least I would like to thank my family, friends, partners of the IFM, and all that people that shared a moment with me during this period. Thanks for all that moments.

Contents

Acronyms

Λ	cosmological constant.
ΛCDM	Cosmological Standard Model.
BAO	Baryonic Acoustic Oscillations.
CDM	Cold Dark Matter.
CMB	Cosmic Microwave Background.
CPL	Chevallier-Polarski-Linder.
DE	Dark Energy.
EoS	Equation of state.
FLRW	Friedmann-Lemaitre-Robertson-Walker.
GR	General Relativity.
HBB	Hot Big Bang.
ISW	Integrated Sachs-Wolfe.
LSS	Last Scattering Surface.
MG	Modified Gravity.
nCPL	Generalized Chevallier-Polarski-Linder.
PPF	Parametrized Post-Friedmannian.
PS	Matter Power Spectrum.
RSD	Redshift-space distortions.
WMAP	Wilkinson Microwave Anisotropy Probe.

Abstract

What is our best current picture of the physical universe, and what are its problems and uncertainties? There is an agreed basic view of the universe, the standard model of cosmology, (ΛCDM), in which the universe expands from a hot big bang early phase to a late-time cool, accelerating phase driven by a cosmological constant, with structure formation. This seems to provide a statistically good fit to all the data up to now, with the same set of parameters, however, there are extensions to it allowed by the same cosmological data sets, in this work, Dark Energy (DE) is modelled by a fluid with an Equation of state (EoS) with time dependency, $w(z)$. Also there are included the effects of dark energy anisotropic stress on features of the matter power spectrum (PS). It is employed the Parametrized Post-Friedmannian (PPF) formalism to emulate an effective DE, and to model its anisotropic stress properties through a two-parameter equation that governs its overall amplitude (g_0) and transition scale (c_g). For the background cosmology, we have considered different equations of state to model DE including a constant w_0 parameter, and models that provide thawing (CPL) and freezing (nCPL) behaviors. We first constrain these parameters by using the Pantheon, BAO, H_0 and Cosmic Microwave Background (CMB) Planck data. Then, it is analyzed the role played by these parameters in the linear Matter Power Spectrum (PS). In order for the anisotropic stress not to provoke deviations larger than 10% and 5% with respect to the ΛCDM PS at $k \sim 0.01\,h/\mathrm{Mpc}$, the parameters have to be in the range $-0.30 < g_0 < 0.32$, $0 \leq c_g^2 < 0.01$ and $-0.15 < g_0 < 0.16$, $0 \leq c_g^2 < 0.01$, respectively.

Keywords: cosmology, dark energy, bayesian statistics.

Resumen

¿Cuál es nuestra mejor descripción actual del universo físico?, y ¿cuáles son sus proplemas e incertidumbres? Existe un modelo que explica como es el universo actualmente, el modelo estándar de la cosmología, (ΛCDM), en el cual, a tiempos tempranos el universo era altamente caliente y comenzó a expandirse y enfriarse a partir de una gran explosión, hasta que actualmente se encuentra en una fase de expansión acelerada, causada por una constante cosmológica. Este modelo es capaz de reproducir y ajustar los datos observacionales usando los mismos parámetros cosmológicos, en este trabajo, la energía oscura (DE) es modelada por un fluido con una ecuación de estado (EoS) dependiente del tiempo, $w(z)$. También se incluyen los efectos que el estrés anisotrópico de la energía oscura puede ocasionar en el espectro de potencias de materia (PS). Es utilizada la Parametrización Post-Friedmanniana (PPF) para simular a la energía oscura e incluir su estrés anisotrópico, para esto se introduce una ecuación con dos parámetros que gobiernan su amplitud (g_0) y su transición de escala (c_g). En cambio, para la cosmología de fondo, la energía oscura ha sido modelada a través de diferentes ecuaciones de estado, incluyendo parametrización constante w_0, y modelos que reproducen comportamientos tipo descongelados (CPL) y congelados (nCPL). Los parámetros fueron ajustados utilizando datos de la muestra de supernovas Pantheon, BAO, H_0 y de radiación cósmica de microondas CMB usando datos de Planck. Después analizamos el papel que estos parámetros juegan en el espectro de potencias de materia PS. Para que el estrés anisotrópico no cause desviaciones más allá del 10% y 5% con respecto al modelo ΛCDM en $k \sim 0.01\,h/\mathrm{Mpc}$, los parámetros tienen que estar en el rango $-0.30 < g_0 < 0.32$, $0 \leq c_g^2 < 0.01$ y $-0.15 < g_0 < 0.16$, $0 \leq c_g^2 < 0.01$, respectivamente.

Palabras clave: cosmología, energía oscura, estadística bayesiana.

Introduction

Fascinated by the night sky the ancient civilizations had the discipline to observe celestial objects: they measured and registered the behavior of the stars to understand and interpret the Universe we live in, the cyclic movements of the sun, moon and planets were inspiration to construct myths and legends about the origin of the universe and also to explain and predict natural phenomena. Explanations about how the universe behaves have been changed according to the available techniques of observation and instruments at each epoch.

The science that studies the Universe: its origin, evolution, geometry, what it is made of and how is the matter distributed is the Cosmology. An extraordinary progress has been made developing cosmological theoretical models and high-precision observational techniques, thanks to it, it was discovered the accelerated expansion of the Universe, the existence of an unknown matter component called dark matter and the large scale distribution of matter.

Nowadays the most accepted cosmological model states that the history of the Universe starts with a Hot Big Bang (HBB), an explosion which occurred everywhere at once, filling all space from the beginning, with an extremely hot and dense plasma of particles and radiation pushing apart from every other particle, electromagnetic radiation was scattered very efficiently by matter. Eventually the Universe cooled to a temperature at which atoms can be formed, lowering the rate of scattering. The HBB era ends when the universe cools enough that matter and radiation, decouple from each other, at this time is defined the Last Scattering Surface (LSS) and since then these photons began to propagate freely through the universe, which is the source of the CMB we detect today. Initially the hot universe was dominated by radiation, later, with cooling from the expansion the roles of matter and radiation changed and the universe entered a matter-dominated era. Recently results suggest that we have already entered an era dominated by dark energy.

The discovery of the accelerated expansion of the Universe implied the existence of dark energy, that has been extensively confirmed by a two-decade variety of experiments, initially employing Supernovae type Ia [1, 2], then using anisotropies in the CMB from WMAP and Planck data [3], distance measurements of different tracers [4], and clustering of large galaxy surveys, among other probes [5, 6, 7]. However, little is known of the fundamental properties of DE, apart from being a 'fluid' that possesses negative pressure. In the most successful model a cosmological constant (Λ), is capable to fit the observations, albeit current tensions exist among a few parameters when measured with different probes [8].

The effects of DE have been widely studied in the context of background cosmological dynamics; most of the work has been devoted to test different equations of state for DE to understand the dynamics of the Hubble expansion flow. However,

in comparison its perturbative effects are less explored, partially because we expect little deviations at perturbative level, but also because we have no clues on its fundamental origin. One can, for example, treat DE as a barotropic fluid, hence, its sound speed depends only on background quantities, or to consider it as a non-adiabatic fluid to account for its linear effects for which additional hypotheses have to be made about the fluid's speed of sound [9]. There are many works that study the effect of DE speed of sound in the perturbative dynamics, initially done by [10, 11, 12, 13]. It turns out that the effects of DE clustering result to be small, especially if the DE EoS is close to -1, as demanded by observations, and then they are difficult to discern with late-Universe measurements [14, 15]. But, in fact, varying the DE sound speed can induce deviations of up 2% in the matter power spectrum (PS) [16], that should be important in view of the expected constraints from upcoming galaxy surveys, such as DESI [17].

Another possibility is to consider DE anisotropic stress. A homogeneous and isotropic symmetric background metric forbids it, but it can be introduced at the perturbed level [18]. Anisotropic stress can also mimic Modified Gravity (MG) at linear order [19, 20, 21, 22], since it introduces at least a new parameter, and together with DE EoS and sound speed, it yields a modified growth of structures in the Universe. In fact, DE stress generates similar outcomes as those of varying the sound speed of DE, but the detailed behavior depends on the signs of the EoS and stress parameter [23]. From theoretical grounds, one expects DE anisotropic stress to affect the evolution of the metric potentials and this provokes CMB temperature anisotropies at low-multipoles, to be affected through the Integrated Sachs-Wolfe (ISW) effect. In Refs. [24, 23, 25, 26, 27, 28] DE anisotropic stress was analyzed to prove this conclusion using CMB data available at that time, but due to the cosmic variance, CMB constraints are still broad. However, DE stress should affect also matter clustering at large scales. Effects of anisotropic stress on the matter power spectrum (PS) and on the growth function have been studied in several works [24, 23, 29, 30, 31, 32, 33], showing that shear viscosity has an effect on very large scales, but one the other hand it does not change much other cosmological parameter values; for instance, for this latter reason we do not expect that DE shear terms alone can alleviate the current tension in the Hubble constant; see however [34] in which it is proven that adding anisotropic shear to interacting models helps to increase the Hubble constant to release the tension for phantom DE.

In the literature there is a number of works considering different aspects of imperfect fluids, e.g. in connection to second order perturbation in ΛCDM [35], or related to generalized scalar fields [36, 37]. Also, based on MG, efforts have been put forward to understand how the gravitational effects of the fifth-force (that generates

an effective shear term) influence the observables at cosmological scales, changing the clustering properties [38, 39]. Our motivation here, linked to these latter works, is to analyze the anisotropic stress effects on CMB and matter PS since the level of accuracy of future LSS galaxy surveys and probes shall demand detailed understanding of the clustering properties of the matter field. In this way, being able to constrain an hypothetical anisotropic shear, stemming either from DE or MG. Ways to carry out this comparison are discussed e.g. in Refs. [40, 41, 42]. Recently, analysis of recent probes hints for non-zero anisotropic stress [43], that also encourages us to further analyze its clustering properties.

In the present work, we use the Parametrized Post-Friedmannian approach [44, 25, 45], though originally motivated to emulate MG models, they naturally introduce an effective DE anisotropic stress term. We consider specific equations of state and fix the DE speed of sound, to concentrate our analysis on the effects of the anisotropic stress. We analyze the constraints from CMB power spectra and, especially, look for deviations in the PS. Interestingly, we find that DE anisotropic stress is allowed by Planck CMB data, as in Refs. [23, 25], but the linear and nonlinear PS impose tighter constraints to it. We consider different DE EoS, firstly $w = -1$ that emulates Λ at background level, then constant w_0, and finally, thawing and freezing models, to find out their effects in combination with stress parameters.

The structure of this thesis is the following: In Chapter 1 is presented a brief resume of Standard Cosmology; including a description about the background dynamics and the linear order perturbed Einstein equations by taking as the background model of the universe on the largest scales the Friedmann-Lemaitre-Robertson-Walker (FLRW) and study the inhomogeneities by considering linear perturbations of the FLRW model: the 'standard model' is such a perturbed FLRW model. In chapter 2 is presented an extension of the ΛCDM model where DE is considered as a fluid with a time depending EoS which can also have perturbations and anisotropic stress, and in Chapter 3 is introduced the PPF formalism to incorporate DE linear perturbations, where a specific anisotropic stress phenomenology is adopted. Chapter 4 shows the results employing different EoS and anisotropic stress considerations. Chapter 5 concludes. Finally, the main results of this thesis were published in the journal Physics of the Dark Universe, [46].

Chapter 1

Standard Cosmology

The standard model of cosmology, ΛCDM, is a testable model that provides a simple and remarkable fit to much of the cosmological data coming from different regions of the visible Universe. This model is based upon a spatially-flat, expanding Universe whose dynamics is governed by General Relativity and whose main matter constituents are baryons, cold dark matter CDM, and a cosmological constant (Λ). The simplicity of this model relies on the fact that it can be well described by six base parameters; cold dark matter density[1] ($\Omega_c h^2$), baryonic density ($\Omega_b h^2$), optical depth (τ), scalar spectral index (n_s), initial amplitude of scalar perturbations (A_s) and the angular size of the sound horizon at recombination (θ_*). These six parameters are fixed to their best-fit values to match several kind of cosmological observations. Also, there are other cosmological parameters derived from these six that help to understand and describe the evolution of the Universe at different times and scale distances such as CMB anisotropies, SNIa, BAO, H_0, RSD, weak lensing of galaxies, galaxy clustering, etc.

The standard ΛCDM model has been well tested both in our local and the late Universe, however this model has some remaining problems, as the cosmological constant origin. There are popular extensions of standard cosmology to provide solutions to specific problems, for example modifications to gravity [47, 48] could give a solution to the cosmological constant origin and also could explain the late time accelerated expansion of the Universe even without a cosmological constant. These theoretical modifications added extra degrees of freedom and should match with the known observations. There are other modifications to ΛCDM and, in this thesis the explored extensions are around the properties of dark energy.

1.1 Background dynamics

At scales larger than about 300 million light years there are no preferred directions in the universe, this means that in average it is equal in all spatial directions around every point on it, this is called isotropy, and also at those scales all the spatial points are equivalent, meaning that there are no special positions so the universe is homogeneous. These assumptions about the universe are the basis of the cosmological principle, and are satisfied by Friedmann-Lemaitre-Robertson-Walker (FLRW) metric, which in spherical coordinates looks like:

$$ds^2 = g_{\mu\nu}dx^\mu dx^\nu = -dt^2 + a^2(t)\left[\frac{dr^2}{1-kr^2} + r^2(d\theta^2 + \sin^2\theta d\phi^2)\right], \tag{1.1}$$

[1] h is defined through $H_0 = 100h$km/s/Mpc

here t is the cosmic time, $a(t)$ the scale factor, k the spatial curvature whose values can represent closed ($k = 1$), flat ($k = 0$) or open ($k = -1$) universes, see Fig.1.1.

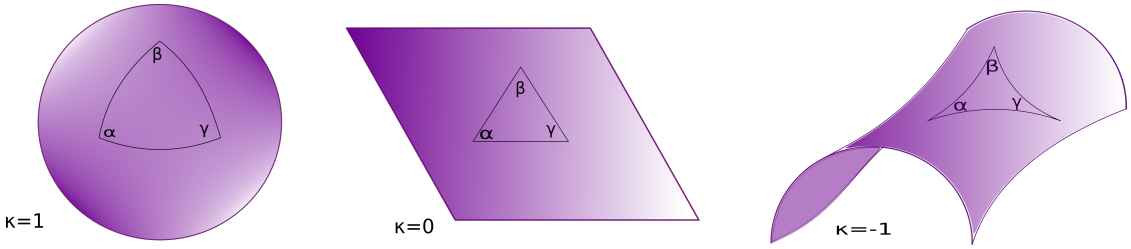

Figure 1.1: Different geometries compatible with cosmological principle. All of them have not frontier, $k = 1$ represents closed, $k = 0$ flat and $k = -1$ open Universes. According to the cosmological data sets the visible Universe is a flat one.

The assumptions on homogeneity and isotropy are compatible with the energy momentum tensor of a perfect fluid:

$$T_{\mu\nu} = (\rho + P)U_\mu U_\nu + P g_{\mu\nu}\,, \tag{1.2}$$

with total density ρ, pressure P, and four-velocity $U^\nu = (1, 0, 0, 0)$, $U_\nu = (-1, 0, 0, 0)$. The dynamics of expansion is obtained using the Einstein field equations:

$$G_{\mu\nu} \equiv R_{\mu\nu} - \frac{1}{2} g_{\mu\nu} R = \frac{8\pi G}{c^4} T_{\mu\nu}. \tag{1.3}$$

along with Eqs.(1.1) and (1.2). Taking the components $\mu\nu = 00$, $\mu\nu = ij$ there are obtained the respective equations:

$$-3\frac{\ddot{a}}{a} = 4\pi G(\rho + 3P)\,, \tag{1.4}$$

$$\frac{\ddot{a}}{a} + 2\left(\frac{\dot{a}}{a}\right)^2 + 2\frac{k}{a^2} = 4\pi G(\rho - P)\,, \tag{1.5}$$

where the dot represents cosmic time derivative, $\dot{} \equiv \frac{d}{dt}$, and double dot second time derivative, substituting $\frac{\ddot{a}}{a}$ from Eq.(1.4) in (1.5) one obtains:

$$\left(\frac{\dot{a}}{a}\right)^2 = \frac{8\pi G}{3}\rho - \frac{k}{a^2}\,, \tag{1.6}$$

this is the fundamental Friedmann equation that governs the expansion of the universe, its left hand side is the square of the Hubble rate, and is common to deal with this equation in terms of H:

$$H \equiv \frac{\dot{a}}{a} \Rightarrow H^2 = \frac{8\pi G}{3}\rho - \frac{k}{a^2}\,. \tag{1.7}$$

The evolution of the Hubble factor depends of the k value, and on what the matter components are and how they evolve. Each matter constituent is described by its own energy momentum tensor, Eq.(1.2) and the conservation law $\nabla^\nu T^{(i)}_{\mu\nu} = 0$ gives the energy density conservation equation for each matter constituent:

$$\dot{\rho}_i + \frac{3\dot{a}}{a}(\rho_i + P_i) = 0 \tag{1.8}$$

where the sub –index i labels the different matter components. To solve this differential equation it is necessary to provide with an equation of state (EoS) that relates pressure with density, $P = P(\rho)$ for barotropic fluids. A popular example of a linear barotropic EoS [2] is:

$$P_i = w_i \rho_i\,, \tag{1.9}$$

w_i is known as EoS parameter, it is usually constant and takes different values for each matter component. The continuity equation Eq.(1.8) can be rewritten in a more known form substituting Eq.(1.9) in it:

$$\dot{\rho}_i = -3H(1 + w_i)\rho_i\,, \tag{1.10}$$

that equation is solved as follows:

$$\frac{1}{\rho_i}\frac{d\rho_i}{dt} = -3\frac{1}{a}\frac{da}{dt}(1 + w_i) \tag{1.11}$$

$$\int d\ln(\rho_i) = -3\int (1 + w_i) d\ln a\,, \tag{1.12}$$

for constant w_i the term $(1 + w_i)$ comes out of the integral:

$$\int d\ln(\rho_i) = -3(1 + w_i)\int d\ln a \tag{1.13}$$

$$\ln\rho_i(a) = -3(1 + w_i)\ln a + cte$$

$$\rho_i(a) = a^{-3(1+w_i)}\mathrm{e}^{cte} \tag{1.14}$$

[2] This equation comes from the pressure definition $P_i \equiv \left(n_i \frac{\partial \rho_i}{\partial n_i} - \rho_i\right)$, and the relation between the density and the number of particles (n_i): $\rho_i = A n_i^\gamma$.

evaluating the last equation at the scale factor today, a_0, gives the density value:

$$\rho_i^0 \equiv \rho_i(a_0) = a_0^{-3(1+w_i)} \mathrm{e}^{cte} \Rightarrow \tag{1.15}$$

$$\mathrm{e}^{cte} = \rho_i^0 a_0^{3(1+w_i)} \tag{1.16}$$

such that,

$$\rho_i(a) = \rho_i^0 \left(\frac{a_0}{a}\right)^{3(1+w_i)} , \tag{1.17}$$

the value of a today is $a_0 = 1$, and finally the density evolution takes the solution:

$$\rho_i(a) = \rho_i^0 a^{-3(1+w_i)} . \tag{1.18}$$

There is an equivalence between the scale factor a and the redshift z:

$$\frac{1}{1+z} = \frac{a(t)}{a_0} = a(t) \tag{1.19}$$

such that $a = 0$ is assigned to the limit $z \to \infty$, and today $z = 0$ corresponds to $a = 1$. All the evolution equations can be written in terms of z instead of a and I will use both representations indistinguishable.

The main constituents of the universe have EoS parameters presented below, and according to Eq. (1.18) its density evolution is also given:

- Baryons: normal matter, after the matter-radiation equality have EoS parameter $w_b = 0$, and density solution; $\rho_b = \rho_b^0 a^{-3}$.
- Cold Dark matter: it is a non relativistic presureless fluid, $w_c = 0$ whose density evolves as: $\rho_c = \rho_c^0 a^{-3}$.
- Radiation: hot relativistic matter with parameter, $w_\gamma = \frac{1}{3}$, the density of photons evolves as $\rho_\gamma = \rho_\gamma^0 a^{-4}$.
- Neutrinos: because of its tiny mass, of utmost 0.1eV, become no relativistic in the late universe, but this effect is not considered in this work. In the era dominated by radiation they are also relativistic with EoS parameter $w_\nu = \frac{1}{3}$ and density solution $\rho_\nu = \rho_\nu^0 a^{-4}$.
- Dark energy: exotic matter represented, in its simplest form, by a cosmological constant, Λ, where $w_\Lambda = -1$ and constant solution, $\rho_\Lambda = \rho_\Lambda^0$.

Using the above specific solutions the Friedmann equation Eq.(1.6) takes the form:

$$H^2(a) = \frac{8\pi G}{3}\left[\rho_\gamma^0 a^{-4} + \rho_\nu^0 a^{-4} + \rho_b^0 a^{-3} + \rho_{dm}^0 a^{-3} + \rho_\Lambda\right] - ka^{-2}\,, \tag{1.20}$$

dividing both sides by H^2:

$$\frac{H^2(a)}{H^2} = \frac{8\pi G}{3H^2}\left[\rho_\gamma^0 a^{-4} + \rho_\nu^0 a^{-4} + \rho_b^0 a^{-3} + \rho_{dm}^0 a^{-3} + \rho_\Lambda\right] - \frac{k}{H^2}a^{-2}\,, \tag{1.21}$$

and considering the definition of the critical density $\rho_{crit} \equiv 3H^2/8\pi G$,

$$\frac{H^2(a)}{H^2} = \frac{\rho}{\rho_{crit}} - \frac{k}{H^2}a^{-2}\,, \tag{1.22}$$

it is also useful to introduce the dimensionless parameter density:

$$\Omega_i \equiv \frac{8\pi G}{3H^2}\rho_i = \frac{\rho_i}{\rho_{crit}}, \quad \Omega_k \equiv -\frac{k}{H^2}a^{-2}\,, \tag{1.23}$$

using these definitions the Hubble parameter is expressed as

$$H(a) = H_0\sqrt{\Omega_\gamma^0 a^{-4} + \Omega_\nu^0 a^{-4} + \Omega_b^0 a^{-3} + \Omega_{dm}^0 a^{-3} + \Omega_k^0 a^{-2} + \Omega_\Lambda}\,. \tag{1.24}$$

From Eq.(1.24) it is clear that each matter component dominates the evolution at different epochs: neutrinos and photons dominate at early times (radiation era) but matter (baryons and CDM) decays in a slower pace than radiation components so eventually it equals the radiation density at the denominated equality epoch and then overcomes it and starts to dominate the evolution (matter era). At more late times dark energy starts to reach the matter density and nowadays it dominates the evolution (dark energy era) of the universe, see Fig.1.2

The Friedmann equation (1.24) also imposes a constraint on the densities evolution, using the critical density definition in Eq.(1.22);

$$1 = \Omega_\gamma + \Omega_\nu + \Omega_b + \Omega_c + \Omega_k + \Omega_\Lambda\,, \tag{1.25}$$

such that the total matter content is always equals to 1, and one of the densities depends on the others and can be expressed in terms of them, for example:

$$\Omega_\Lambda = 1 - (\Omega_\gamma + \Omega_\nu + \Omega_b + \Omega_c + \Omega_k)\,. \tag{1.26}$$

Diverse cosmological probes will constrain these density parameters evaluated at present times.

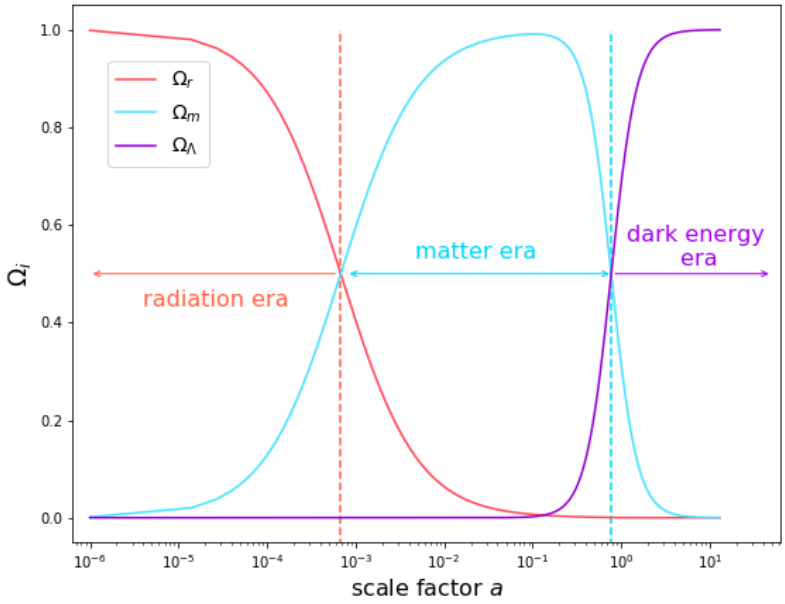

Figure 1.2: Densities evolution, for $k = 0$ and according Eq.(1.24) there are radiation, matter and dark energy eras with $\Omega_r = \Omega_\gamma + \Omega_\nu$, $\Omega_m = \Omega_b + \Omega_c$.

1.1.1 Luminosity distances

Distant luminosity sources radiate isotropically, at different distances from it, the flux tends to diminish at larger distances, R, from the source but the total energy is conserved at each surface area of an sphere of radius R, see Fig.1.3. In an expanding universe the luminosity distance d_L that travels an emitted photon is related to the comoving distance R by the relation $d_L = (1+z)R$. For the FLRW metric Eq.(1.1) the luminosity distance is computed as:

$$d_L = \frac{(1+z)}{H_0} \frac{c}{\sqrt{|\Omega_k^0|}} \text{sinn}\left[\sqrt{|\Omega_k^0|}\int_0^z \frac{dz'}{E(z')}\right], \tag{1.27}$$

where

$$E(z) = \frac{H(z)}{H_0}, \tag{1.28}$$

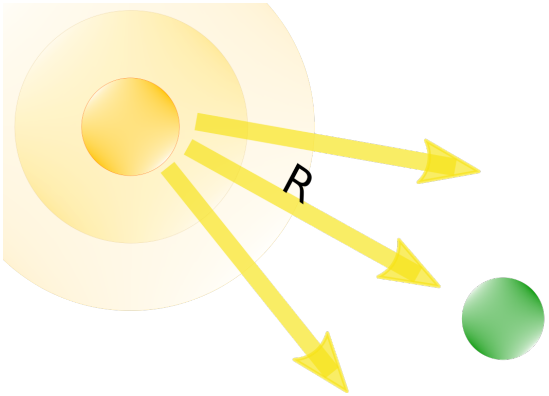

Figure 1.3: The flux received by an observer depends on its comoving distance, R, to the brilliant source.

and

$$\text{sinn}\left[\sqrt{|\Omega_k^0|}\int_0^z \frac{dz'}{E(z')}\right] = \begin{cases} \sin\left[\sqrt{|\Omega_k^0|}\int_0^z \frac{dz'}{E(z')}\right] & \text{for} \quad \Omega_k < 0\,, \\ \left[\sqrt{|\Omega_k^0|}\int_0^z \frac{dz'}{E(z')}\right] & \text{for} \quad \Omega_k = 0\,, \\ \sinh\left[\sqrt{|\Omega_k^0|}\int_0^z \frac{dz'}{E(z')}\right] & \text{for} \quad \Omega_k > 0\,. \end{cases} \tag{1.29}$$

On the other hand, there is also another way to measure distances in cosmology, objects with physical size D are viewed at δ angles, see Fig.1.4, the relation between these quantities,valid for small angles, $d_A = \frac{D}{\delta}$, is known as the angular diameter distance, and is related to the luminosity distance through the equation:

$$d_A = \frac{d_L(z)}{(1+z)^2}\,. \tag{1.30}$$

Other cosmological distances are functions of integrals of the Hubble parameter, so at the background level Eq, (1.24) is the most relevant equation that must be found.

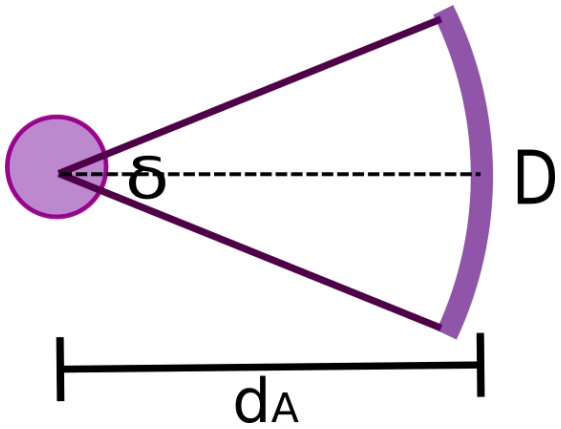

Figure 1.4: The physical size of an object, D is subtended by a angle δ, if the distance, d_A, between the object and the observer. Larger distances d_A to the same object yields smaller angles, δ, and if $d_A \gg D$ then $d_A = \frac{D}{\delta}$.

1.1.2 Dark energy

The discovery of the accelerated expansion of the Universe implied the existence of dark energy, that has been extensively confirmed by a two-decade variety of experiments, initially employing Supernovae type Ia [1, 2], and thereafter a lot of distinct astronomical observations as Baryonic acoustic oscillations distance measurements, galaxy clusters [5, 6, 7] and recent measurements of the Hubble factor H_0 [49, 8], those are known as background observations and are well fitted by the ΛCDM model.

- **Supernovas Ia** are standard candles which means that if they have identical color, shape and neighborhood then, on average, they also have the same intrinsic luminosity, and the "observed" modulus distance is computed by the model:

$$\mu^{obs} = m_B^\star - (M_B - \alpha X_1 + \beta C)\,, \tag{1.31}$$

  where $m_B^\star$ is the observed magnitude peak in the rest frame of the Supernova, X_1 is the time stretching, B the color band, α, β and M_B are *nuisance* parameters that depend on the host galaxy properties. For the compilation JLA [50] this nuisance parameters have to be incorporated as free parameters and for the combined Pantheon sample [51] those are not free parameters and are fixed to 0. The light curve parameters $(m_B^\star, X_1, C)$ are fitted using parameter reconstruction models (e.g. SALT2 [52], SiFTO [53], SNANA [54]) along with photometrical data.

  Flux measurements allow to establish a relation between the apparent and absolute magnitude of an object which it is known as the distance modulus:

$$\mu(z) = m(z) - M \tag{1.32}$$

  and it has the equation

$$\mu(z) = 5\log_{10}\left(\frac{d_L(z)}{10\text{pc}}\right) + 25\,, \tag{1.33}$$

  d_L is calculated using Eq.(1.27). This theoretical equation depends on the density parameter values and they have to be fitted using the observational data Eq.(1.31) and Bayesian statistical techniques.

- **Baryonic acoustic oscillation (BAO)** is an early time phenomenon originated by the competing forces of radiation pressure and gravity which set up oscillations in the photon-baryon fluid. Those perturbations propagate outwards as acoustic waves and imprinted a characteristic scale, the sound horizon

r_s, in the spatial distribution of cosmic objects. Distance measurements come from galaxy catalogues where, using the imprint of the early sound waves, it is possible to measure the distance to these galaxies using a geometrical test, namely the angular extent of a feature of known size.

The expansion of the universe using BAO observations, usually is through the angular diameter distance Eq.(1.30), and there are different data sets available [55, 56, 57, 58].

- **Hubble factor:** today's expansion rate, H_0, can be predicted using late time observations. The methods to measure this parameter require to build a "distance ladder" using geometry to calibrate the luminosities of standarizable star types; for example, cepheid variables are pulsating stars whose period of variation strongly correlates with their luminosities, such that cepheids with the same period also have the same magnitude absolute; the other independent measurements come from SN Ia, which can be seen at greater distances than cepheids. This kind of observations must be fitted with equation (1.24).

These types of cosmological observations can be used together or independently to put constraints on the ΛCDM background model parameters, $(\Omega_m, \Omega_\Lambda, \Omega_k, H_0)$, combined constraints from SNIa, BAO, and H_0 measurements are shown in Tab.1.1 and in Fig.1.5. According to these results, the 32% of the total matter in the universe

Parameter	68% limits
Ω_m	0.307 ± 0.017
Ω_Λ	0.683 ± 0.025
Ω_K	0.0107 ± 0.0088
H_0	74.0 ± 1.4

Table 1.1: ΛCDM model background parameter constraints at 68%, using SNIa, BAO and H_0 observations.

is made of neutrinos, photons, baryonic and dark matter, nevertheless the 68% is dark energy emulated here by a cosmological constant Λ, and open universes ($\Omega_k > 0$) are favored but in the contour plots for Ω_k is appreciated that flat and closed universes are inside of the 68, 95 and 99% confidence limits. More tightly parameter constraints are imposed when early time observations are considered in the analysis.

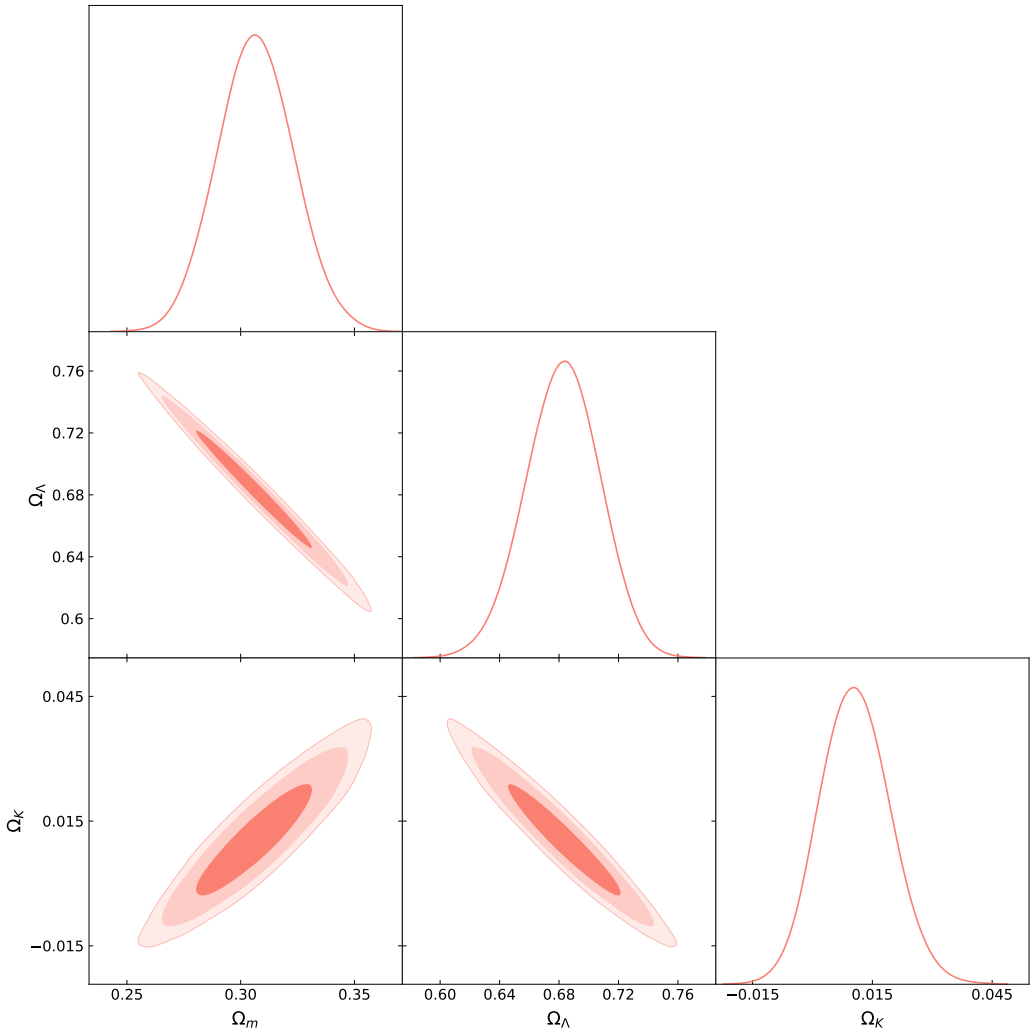

Figure 1.5: ΛCDM model constraints (68%, 95% and 99% confidence limits) on density parameters Ω_m, Ω_Λ and Ω_k, using SNIa [51], BAO[59] and H_0 [8] measurements.

1.2 Linear perturbation theory

Late time cosmological observations can be well described by the FLRW metric, where the assumptions on homogeneity and isotropy holds. This is not totally true for early time cosmological observations as the CMB, where the distribution of temperature has small deviations from a central value, and so the matter distribution is not homogeneous. Those disturbances can be described by the theory of small fluctuations where tensorial quantities can be expressed as its mean value plus small deviations around it [60] as follows:

$$T(t, x^i) = T_0(t) + \delta T(t, x^i)\,, \tag{1.34}$$

t is the cosmic time, $T_0(t)$ is the average value of T. In cosmology, those quantities are known as the background values for which the cosmological principle is still valid, so they only depends on time. $\delta T(t, x^i)$ are the fluctuations, which depend also on spatial coordinates and can be expressed as power series:

$$\delta T(t, x^i) = \sum_{n=1}^{\infty} \frac{\epsilon^n}{n!} \delta T_n(t, x^i)\,, \tag{1.35}$$

the subscript n denotes the order of the perturbations, and ϵ is a small parameter of expansion. Since equations of General Relativity are tensorial, the perturbed spacetime can be described using this generic expansion, to arrive to the perturbed Einstein's equations is necessary to consider metric and matter perturbations.

• **Metric perturbations.**

The spacetime metric is represented by a symmetric tensor, $g_{\mu\nu} = g_{\nu\mu}$, which following Eqs.(1.34),(1.35) can be written as:

$$g_{\mu\nu} = g^0_{\mu\nu} + \epsilon \delta g_{\mu\nu} + \epsilon^2 \frac{1}{2} \delta^2 g_{\mu\nu} + \dots\,, \tag{1.36}$$

$g^0_{\mu\nu}$ is the unperturbed FLRW metric Eq.(1.1), $\epsilon \delta g_{\mu\nu} \equiv h_{\mu\nu}$ is the first order perturbation, $\epsilon^2 \frac{1}{2} \delta^2 g_{\mu\nu}$ is the second order one, etc. The goal of this section is to describe only the first order perturbations, also called linear perturbation theory, and the metric follows the next notation,

$$g_{\mu\nu} = g^0_{\mu\nu} + h_{\mu\nu}\,. \tag{1.37}$$

Perturbations can be decoupled into scalar, vector and tensor modes, according to their properties under spatial coordinate transformations. Scalar perturbations

are invariant under rotations, while vector and tensor fluctuations transform like vectors and tensors under spatial rotations. The components of the perturbed metric, time-time linear–order behaves as a scalar, time-space like a spatial vector and the spatial–spatial as a spatial tensor.

According to the Helmholtz theorem, spatial vectors $\mathcal{U}_i$ can be decomposed into a further scalar component, $\mathcal{U}^S$, and a purely vector component, $\mathcal{U}_i^{\rm V}$;

$$\mathcal{U}_i \equiv \frac{\partial \mathcal{U}^S}{\partial x^i} + \mathcal{U}_i^{\rm V}\,, \tag{1.38}$$

where $\mathcal{U}_i^V$ is a divergence free vector, $\dfrac{\partial \mathcal{U}_i^V}{\partial x^i} = 0$.

Similarly the spatial–spatial components of a symmetric two rank tensor, $\mathcal{T}_{ij}$, can be decomposed into a purely scalar, vector and tensor components:

$$\mathcal{T}_{ij} = \mathcal{T}^S \delta_{ij} + \frac{\partial^2 \mathcal{S}}{\partial x^i \partial x^j} + \frac{\partial \mathcal{T}_i^V}{\partial x^j} + \frac{\partial \mathcal{T}_j^V}{\partial x^i} + \mathcal{T}_{ij}^T\,, \tag{1.39}$$

$\mathcal{T}_{ij}^T$, $\mathcal{T}_i^V$, $(\mathcal{T}^S, \mathcal{S})$ are respectively tensor, vector and scalar type components of the tensor $\mathcal{T}_{ij}$. The conditions on these components are that the divergence of vector and tensor modes is null, $\dfrac{\partial \mathcal{T}_i^V}{\partial x^i} = \dfrac{\partial \mathcal{T}_{ij}^T}{\partial x^i} = 0$, and the tensor component is trace free $\mathcal{T}_{ii}^T = 0$.

In this framework, using Eqs.(1.38)-(1.39) one can decompose perturbations of various quantities into three types of components: scalar, vector and tensor. At linear order there is no coupling between the different fluctuation modes and they can be studied independently. Following this prescription, the components of the first–order metric perturbation $h_{\mu\nu}$ can be decomposed as follows:

$$h_{tt} = -2A\,, \tag{1.40}$$

$$h_{it} = a\left[\frac{\partial B}{\partial x^i} + G_i\right]\,, \tag{1.41}$$

$$h_{ij} = a^2\left[2H_L\delta_{ij} + 2\frac{\partial^2 H_T}{\partial x^i \partial x^j} + \frac{\partial C_i}{\partial x^j} + \frac{\partial C_j}{\partial x^i} + D_{ij}\right]\,, \tag{1.42}$$

where A, B, H_L, H_T are the four scalar metric perturbations, C_i and G_i are divergenless vector modes and D_{ij} is a trace-free and divergenless tensor perturbation,

$$\frac{\partial C_i}{\partial x^i} = \frac{\partial G_i}{\partial x^i} = 0, \qquad \frac{\partial D_{ij}}{\partial x^i} = 0, \qquad D_{ii} = 0\,, \tag{1.43}$$

using this conditions the trace of the perturbed metric has only scalar modes,

$$h_{ii} = a^2 \left[6H_L + 2\nabla^2 H_T\right] . \tag{1.44}$$

• **Energy-momentum perturbations.**

Using the same framework the energy momentum tensor can be expressed as a background tensor, $T^0_{\mu\nu}$, plus small perturbations around it,

$$T_{\mu\nu} = T^0_{\mu\nu} + \delta T_{\mu\nu} + \dots , \tag{1.45}$$

each matter component has its own energy momentum tensor according to their properties, if the fluids are perfect fluids at the background level they are described by the equation (1.2). For an imperfect fluid, the stress–energy tensor must include extra terms corresponding in a weakly collisional gas to shear and bulk viscosity, thermal conduction, and other physical processes, these properties are included by the addition of an extra traceless tensor, $\Sigma_{\mu\nu}$,

$$T_{\mu\nu} = (\rho + P)U_\mu U_\nu + P g_{\mu\nu} + \Sigma_{\mu\nu} , \tag{1.46}$$

and its first–order perturbation yields,

$$\delta T_{\mu\nu} = (\delta P)\, g^0_{\mu\nu} + P^0 h_{\mu\nu} + (\delta\rho + \delta P)\, U^0_\mu U^0_\nu + \left(\rho^0 + P^0\right) \left[(\delta U_\mu)U^0_\nu + U^0_\mu(\delta U_\nu)\right] + \Sigma_{\mu\nu} , \tag{1.47}$$

to split $\delta T_{\mu\nu}$ by components it is necessary to substitute the metric and velocity ones. Considering that the total four–velocity satisfies the relation:

$$U_\nu U^\nu = -1 \Longrightarrow g^{\mu\nu} U_\mu U_\nu = -1 , \tag{1.48}$$

and taking the first order perturbation of the last equation:

$$h^{\mu\nu} U^0_\mu U^0_\nu + g^{\mu\nu}_0 \left[(\delta U_\mu)U^0_\nu + U^0_\mu(\delta U_\nu)\right] = 0 , \tag{1.49}$$

the time–time component of the previous equation gives,

$$h^{tt} U^0_t U^0_t + g^{tt}_0 \left[(\delta U_t)U^0_t + U^0_t(\delta U_t)\right] = 0 , \tag{1.50}$$

$$h^{tt} + 2\delta U_t = 0 , \tag{1.51}$$

finally the time perturbed velocity takes the form:

$$\delta U_t = -\frac{1}{2} h^{tt} = \frac{1}{2} h_{tt} . \tag{1.52}$$

The spatial perturbed velocity component, δU_i, is commonly written as v_i that can be decomposed as an spatial vector according to Eq.(1.38):

$$v_i \equiv \delta U_i = \frac{\partial \delta U^S}{\partial x^i} + \delta U_i^V, \quad \frac{\partial \delta U_i^V}{\partial x^i} = 0\,. \tag{1.53}$$

Replacing the decomposition of the perturbed velocity in Eq.(1.47) there are obtained the equations,

$$\begin{aligned}
\delta T_{tt} &= -\delta P + P^0 h_{tt} + \delta\rho + \delta P + \left(\rho^0 + P^0\right)\left[-h_{tt}\right] \\
&= -\rho h_{tt} + \delta\rho\,, \qquad (1.54)\\
\delta T_{ti} &= P^0 h_{ti} + \left(\rho^0 + P^0\right)\left[U_t^0(\delta U_i)\right] \\
&= P^0 h_{ti} - \left(\rho^0 + P^0\right)\left[\frac{\partial(\delta U^S)}{\partial x^i} + \delta U_i^V\right], \qquad (1.55)\\
\delta T_{ij} &= a^2\delta_{ij}(\delta P) + P^0 h_{ij} + a^2\Sigma_{ij}\,, \qquad (1.56)\\
\delta T_{ii} &= 3a^2\delta P + P^0 h_{ii} + a^2\Sigma_{ii}\,, \qquad (1.57)
\end{aligned}$$

it is usual to define a dimensionless version of the anisotropic stress by $\Pi_{ij} \equiv \Sigma_{ij}/P$ whose decomposition as a spatial tensor is:

$$\begin{aligned}
\Pi_{ij} &= \frac{1}{3}\delta_{ij}\nabla^2\Pi - \frac{\partial^2\Pi}{\partial x^i \partial x^j} + \frac{\partial \Pi_i^V}{\partial x^j} + \frac{\partial \Pi_j^V}{\partial x^i} + \Pi_{ij}^T\,, \\
\frac{\partial \Pi_i^V}{\partial x^i} &= \frac{\partial \Pi_{ij}^T}{\partial x^i} = \Pi_{ii}^T = 0\,. \qquad (1.58)
\end{aligned}$$

It is useful to have in mind that contracted components of the energy momentum tensor can be obtained by using the equation,

$$\delta T_\nu^\mu = h^{\mu\beta} T^0_{\beta\nu} + g_0^{\mu\beta}\delta T_{\beta\nu}\,. \tag{1.59}$$

Using this expression, is possible to work out Eq.(1.45) to first order:

$$\begin{aligned}
T^0{}_0 &= -\left(\rho + \delta\rho\right), \\
T^0{}_k &= \left(\rho + P\right) v_k, \\
T^k{}_l &= \left(P + \delta P\right)\delta^k{}_l + P\Pi^k{}_l, \qquad (1.60)
\end{aligned}$$

1.2.1 Perturbed Einstein equations

There are different ways to arrive to the first–order perturbed Einstein equations $\delta G_{\mu\nu}$, the goal of this subsection is only give some of the main steps to do it, for a

further derivation you can consult [61, 62]. One way is to start perturbing both sides of Eq.(1.3) and then separate the background from the linear order, another way is first to substitute R by $-\kappa T^3$ in Eq.(1.3) and then perturbs the equivalent equation as follows,

$$R_{\mu\nu} = \kappa T_{\mu\nu} - \frac{1}{2}\kappa g_{\mu\nu} T \,, \tag{1.61}$$

$\kappa = \frac{8\pi G}{c^4}$, and $c = 1$. The total Ricci tensor, the stress and the metric tensor, Eq.(1.61), can be written as background plus a perturbed part,

$$R^0_{\mu\nu} + \delta R_{\mu\nu} = \kappa T^0_{\mu\nu} - \frac{1}{2}\kappa g_{\mu\nu} T^0 + \kappa \delta T_{\mu\nu} - \frac{1}{2}\kappa (h_{\mu\nu}) T^0 - \frac{1}{2}\kappa g_{\mu\nu}\delta T \,, \tag{1.62}$$

the background has the solutions described in previous sections and can be separated from the first–order perturbed equations because they are not coupled, the linear equations are,

$$\delta R_{\mu\nu} = \kappa \delta T_{\mu\nu} - \frac{1}{2}\kappa (h_{\mu\nu}) T^0 - \frac{1}{2}\kappa g_{\mu\nu}\delta T \,, \tag{1.63}$$

the left hand side involves only geometrical quantities and it's components are given in terms of metric perturbations as;

$$\begin{aligned} \delta R_{tt} &= -\frac{1}{2a^2}\left(\nabla^2 h_{tt}\right) - \frac{3}{2}\left(\frac{\dot{a}}{a}\right)\dot{h}_{tt} + \frac{1}{a^2}\partial_i \dot{h}_{it} \\ &\quad -\frac{1}{2a^2}\left[\ddot{h}_{ii} - 2\left(\frac{\dot{a}}{a}\right)\dot{h}_{ii} + 2\left(\left(\frac{\dot{a}}{a}\right)^2 - \frac{\ddot{a}}{a}\right)h_{ii}\right] \,, \end{aligned} \tag{1.64}$$

$$\begin{aligned} \delta R_{ti} &= -\left(\frac{\dot{a}}{a}\right)\partial_i h_{tt} - \frac{1}{2a^2}\left(\nabla^2 h_{ti} - \partial_i \partial_j h_{tj}\right) + \left[\frac{\ddot{a}}{a} + 2\left(\frac{\dot{a}}{a}\right)^2\right] h_{ti} \\ &\quad -\frac{1}{2}\partial_t\left[\frac{1}{a^2}\left(\partial_i h_{jj} - \partial_j h_{ji}\right)\right] \,, \end{aligned} \tag{1.65}$$

$$\begin{aligned} \delta R_{ij} &= \frac{1}{2}\partial_i\partial_j h_{tt} + \left(2\dot{a}^2 + a\ddot{a}\right)\delta_{ij} h_{tt} + \frac{1}{2}a\dot{a}\delta_{ij}\dot{h}_{tt} \\ &\quad -\frac{1}{2a^2}\left(\nabla^2 h_{ij} - \partial_k\partial_i h_{kj} - \partial_k\partial_j h_{ki} + \partial_i\partial_j h_{kk}\right) + \frac{1}{2}\ddot{h}_{ij} \\ &\quad -\frac{\dot{a}}{2a}\left(\dot{h}_{ij} - \delta_{ij}\dot{h}_{kk}\right) - \left(\frac{\dot{a}}{a}\right)^2\left[-2h_{ij} + \delta_{ij}h_{kk}\right] - \frac{\dot{a}}{a}\delta_{ij}\partial_k h_{kt} \\ &\quad -\frac{1}{2}\left(\partial_i \dot{h}_{jt} + \partial_j \dot{h}_{it}\right) - \frac{\dot{a}}{2a}\left(\partial_i h_{jt} - \partial_j h_{it}\right) \,, \end{aligned} \tag{1.66}$$

[3]Contracting Einstein equation: $g^{\mu\nu}\left(R_{\mu\nu} - \frac{1}{2}g_{\mu\nu}R = \kappa T_{\mu\nu}\right) \Rightarrow R = -\kappa T$

$$\begin{aligned}\delta R_{ii} &= \frac{1}{2}\nabla^2 h_{tt} + (2\dot{a}^2 + a\ddot{a})3h_{tt} + \frac{3}{2}a\dot{a}\dot{h}_{tt} - \frac{1}{2a^2}\left(2\nabla^2 h_{ii} - 2\partial_k\partial_i h_{ki}\right) \\ &\quad + \frac{1}{2}\ddot{h}_{ii} + \frac{\dot{a}}{a}\dot{h}_{ii} - \frac{\dot{a}^2}{a^2}h_{ii} - 3\frac{\dot{a}}{a}\partial_k h_{kt} - \partial_i\dot{h}_{it}\,. \end{aligned} \tag{1.67}$$

The Einstein field equations relate perturbations in the metric to perturbations in the matter through Eq.(1.63). Taking components and replacing the generic decomposition of the perturbed metric and stress tensor we found equations that govern the evolution of metric perturbations. This derivation can be done considering only scalar, vector or tensor components.

When only scalar fluctuations are considered and combining the different components of the Einstein equations, and changing time derivatives[4] by derivatives with respect to $' = d/ln(a)$ it is possible to write the usual system of equations in Fourier space:

$$H_L + \frac{1}{3}H_T + \frac{B}{k_H} - \frac{H_T'}{k_H^2} = \frac{4\pi G a^2}{k^2}\left[\delta\rho + 3aH(\rho+P)\frac{(v-B)}{k}\right], \tag{1.68}$$

$$A + H_L + \frac{H_T}{3} + \frac{B' + 2B}{k_H} - \left[\frac{H_T''}{k_H^2} + \left(3 + \frac{H'}{H}\right)\frac{H_T'}{k_H^2}\right] = -\frac{8\pi G a^2}{k^2}P\Pi\,, \tag{1.69}$$

$$A - H_L' - \frac{H_T'}{3} = \frac{4\pi G a}{H}(\rho+P)\frac{v-B}{k}\,, \tag{1.70}$$

$$A' + \left(2 + 2\frac{H'}{H} - \frac{k_H^2}{3}\right)A - \frac{k_H}{3}(B' + B) - H_L'' - \left(2 + \frac{H'}{H}\right)H_L' \tag{1.71}$$

$$= \frac{4\pi G}{H^2}\left(\delta P + \frac{1}{3}\delta\rho\right), \tag{1.72}$$

where $\delta\rho, \delta P$, $P\Pi$ are the sum of individual matter components.

$$\begin{aligned}\delta\rho = \sum_a \delta\rho_a, \quad \delta P = \sum_a \delta P_a, \quad P\Pi = \sum_a P_a\Pi_a, \\ (\rho+P)\frac{v-B}{k} = \sum_a (\rho_a + P_a)\frac{v_a - B_a}{k}\end{aligned} \tag{1.73}$$

Although we know the Einstein equations, it is helpful to derive the first order perturbation of the continuity, $\nabla_\mu T^{\mu 0}$, and Euler equations, $\nabla_\mu T^{\mu i}$. These perturbations

[4] $\dot{x} = Hx'$

give the energy and momentum conservation equations for each non interacting matter component:

$$\delta\rho_a' + 3(\delta\rho_a + \delta P_a) = -(\rho_a + P_a)(k_H v_a + 3H_L'), \tag{1.74}$$

$$\frac{[a^4(\rho_i + P_a)(v_a - B)]'}{a^4 k_H} = \delta P_i - \frac{2}{3} P_a \Pi_a + (\rho_a + P_a)A\,. \tag{1.75}$$

These equations hold for each individual component and are solved together with equations (1.68)-(1.72). The evolution equations derived in the previous subsections can be solved numerically once the initial conditions are specified, for this is useful to work in different gauges (see next sections).

1.2.2 Gauge freedom

A physical space–time can be characterized by different metrics and coordinate systems. They are chosen according to the properties of the physical system under consideration. In cosmology, the preferred background metric is the FLRW metric that can be written in spherical or rectangular coordinates. However, when perturbations are considered it is possible to go from the background to the perturbed metric using a correspondence rule, this is referred to as a gauge. This map is not unique and is generated by a vector field, the gauge generator.

Perturbed modes can be obtained using different diffeomorphisms, $\phi : M \longrightarrow N$, between manifolds, some of them introduce quantities without physical meaning, however it is possible to describe the universe by choosing specific observers for which the perturbed equations have a physical interpretation.

There are two approaches to calculate how perturbations change under a small coordinate or gauge transformation. In the **passive** view there is a transformation rule between two coordinate systems which allows to study the behavior of the perturbations under this transformation rule. In the **active** approach it is considered the one–parameter family of diffeomorphisms, $\phi_\tau : M \longrightarrow M$, generated by a vector field V^α, that allows to compare a given tensor field, $\tilde{T}$, with the new tensor field T that arises from the action of ϕ^5 using the notion of the Lie derivative with respect to the vector field V^α: $\tilde{T} = T - \mathcal{L}_V T^{(0)}$. For the metric tensor it yields,

$$\tilde{h}_{\mu\nu} = h_{\mu\nu} - \mathcal{L}_V[g^0_{\mu\nu}]\,, \tag{1.76}$$

the Lie derivative of the metric is:

$$\mathcal{L}_V[g^0_{\mu\nu}] = \nabla^0_\mu V_\nu + \nabla^0_\nu V_\mu\,, \tag{1.77}$$

where,

$$\nabla^0_\mu V_\nu = \partial_\mu V_\nu - \Gamma^\alpha_{\mu\nu} V_\alpha\,,$$

such that the transformation between perturbed metrics is given by the expression:

$$\tilde{h}_{\mu\nu} = h_{\mu\nu} - (\partial_\mu V_\nu + \partial_\nu V_\mu - 2\Gamma^\alpha_{\mu\nu} V_\alpha)\,. \tag{1.78}$$

the vector field $V_\alpha = (V_t, V_i)$ has time and vector components, the time component V_t behaves as a scalar, and the vector component, V_i, decomposes into a scalar plus a vector part,

$$V_i = \partial_i V^S + V^V_i\,. \tag{1.79}$$

[5] $\tilde{T} = \phi^*_\tau T$

Using Eq.(1.78) and replacing the decomposition of the gauge generator Eq.(1.79) we obtained the transformation rules of the time–time, time–space and space–space perturbed components of the metric:

$$\tilde{h}_{tt} = h_{tt} - (2\partial_t V_t + -2\Gamma^{\alpha}_{tt} V_\alpha) = h_{tt} - 2\partial_t V_t \,, \tag{1.80}$$

$$\tilde{h}_{ti} = h_{ti} - (\partial_t V_i + \partial_i V_t - 2\Gamma^{j}_{ti} V_j) = h_{ti} - \partial_t V_i - \partial_i V_t + 2\frac{\dot{a}}{a} V_i \tag{1.81}$$

$$\tilde{h}_{ij} = h_{ij} - (\partial_i V_j + \partial_j V_i - 2\Gamma^{t}_{ij} V_t) = h_{ij} - \partial_i V_j - \partial_j V_i + 2a\dot{a}\delta_{ij} V_t \,, \tag{1.82}$$

replacing the decomposition of the metric components Eqs.(1.40)-(1.42):

$$-2\tilde{A} = -2A - 2\partial_t V_t \Rightarrow \tilde{A} = A + \partial_t V_t \tag{1.83}$$

$$a[\partial_i \tilde{B} + \tilde{G}_i] = a[\partial_i B + G_i] - \partial_t[\partial_i V^S + V^V_i] - \partial_i V_t + 2\frac{\dot{a}}{a}[\partial_i V^S + V^V_i] \tag{1.84}$$

the proportional part of ∂_i yields the transformation rule of the scalar component B,

$$\tilde{B} = B - \frac{1}{a}\left(\partial_t V^S + V_t - 2HV^S\right) \,, \tag{1.85}$$

and the vector component yields the transformation of the vector component G_i,

$$\tilde{G}_i = G_i + \frac{1}{a}\left(-\partial_t V^V_i + 2HV^V_i\right) \tag{1.86}$$

and finally for the space–space transformation:

$$a^2\left[2\tilde{H}_L\delta_{ij} + \frac{2\partial^2\tilde{H}_T}{\partial x^i\partial x^j} + \frac{\partial\tilde{C}_i}{\partial x^j} + \frac{\partial\tilde{C}_j}{\partial x^i} + \tilde{D}_{ij}\right] = a^2\left[2H_L\delta_{ij} + \frac{2\partial^2 H_T}{\partial x^i\partial x^j} + \frac{\partial C_i}{\partial x^j}\right.$$
$$\left. + \frac{\partial C_j}{\partial x^i} + D_{ij}\right] - \partial_i[\partial_j V^S + V^V_j] - \partial_j[\partial_i V^S + V^V_i] + 2a\dot{a}\delta_{ij} V_t \,, \tag{1.87}$$

taking the proportional parts of δ_{ij}, $\partial_i\partial_j$, ∂_i and of the tensor part we have,

$$\tilde{H}_L = H_L + HV_t \,, \tag{1.88}$$

$$\tilde{H}_T = H_T - \frac{1}{a^2} V^S \,, \tag{1.89}$$

$$\tilde{C}_i = C_i - \frac{1}{a^2} V^V_i \,, \tag{1.90}$$

$$\tilde{D}_{ij} = D_{ij} \,. \tag{1.91}$$

In other notations, the temporal component of the vector field is denoted by α and the scalar part of the space component V^S by β.

The active approach can be used also to obtain the transformation rules of the energy momentum tensor:

$$\delta\tilde{T}_{\mu\nu} = \delta T_{\mu\nu} - \mathcal{L}_V T^0_{\mu\nu}\,, \tag{1.92}$$

and for the energy density and pressure it yields:

$$\tilde{\delta\rho} = \delta\rho + \mathcal{L}_V \rho^0 \Rightarrow \tilde{\delta\rho} = \delta\rho + V_t \dot{\rho}^0\,, \tag{1.93}$$

$$\delta\tilde{P} = \delta P + \mathcal{L}_V P^0 \Rightarrow \delta\tilde{P} = \delta P + V_t \dot{P}^0\,. \tag{1.94}$$

Using these prescriptions it is possible to go from the equations in one gauge to another one. Historically many gauges have been used and for different times in the evolution of the Universe, different gauges have their advantages. Cosmological codes [63] are usually written (and solved) in synchronous gauge [64] because the equations are better behaved numerically in that gauge. It is common to work the theoretical equations in another gauge and then make the correspondent changes to synchronous. A further discussion between Newtonian and synchronous gauge can be consulted in [64]. In this work the main equations are given in Newtonian and matter comoving gauge.

1.2.3 Newtonian gauge

This metric (N) is generated by choosing the components of the vector field, V_N^S and V_t^N such that $H_T = 0$ and $B = 0$,

$$V_N^S = -a^2 \tilde{H}_T, \quad V_t = -a\tilde{B} + a^2 \dot{\tilde{H}}_T \,, \tag{1.95}$$

replacing these particular solutions, V_N^S, V_t^N, in Eqs.(1.85)-(1.91) there are obtained the transformation rules between perturbed tensors in different gauges to Newtonian. In Newtonian gauge it is conventional to rewrite the scalar metric potentials as:

$$H_L = \Phi, \quad \Psi = A, \quad B = H_T = 0 \,. \tag{1.96}$$

The total metric in conformal Newtonian, longitudinal gauge is given by the equation,

$$ds^2 = a^2(\tau) \left[-(1+2\Psi)\, d\tau^2 + (1+2\Phi) dx^i dx_i \right] , \tag{1.97}$$

where Ψ and Φ are gauge invariant scalar potentials [65, 66], Φ is called the Newtonian potential since it has evolution equations closest to the Newtonian ones. In this metric the components of the energy momentum tensor are

$$\begin{aligned} T^0{}_0 &= -(\rho + \delta\rho) \,, \\ T^0{}_k &= (\rho + P)\, v_k, \\ T^k{}_l &= (P + \delta P)\, \delta^k{}_l + P \Pi^k{}_l, \end{aligned} \tag{1.98}$$

where ρ and P are the background energy density and pressure, $\delta\rho$ and δP their respective perturbations, and $\Pi^k{}_l$ are the anisotropic stress components. Since we are dealing with scalar perturbations, it is useful to work with the velocity divergence θ and the scalar anisotropic stress Π defined as

$$\theta = i k^i v_i, \tag{1.99}$$

$$\Pi = -\frac{3}{2} \left(\frac{k_i k_j}{k^2} - \frac{1}{3} \delta_{ij} \right) \Pi^{ij}. \tag{1.100}$$

The Einstein's field equations, in this metric are

$$k^2 \Phi = 4\pi G a^2 \sum_{\mathrm{a}} \left(\delta\rho_{\mathrm{a}} + 3Ha(\rho_{\mathrm{a}} + P_{\mathrm{a}}) \frac{\theta_{\mathrm{a}}}{k^2} \right) \,, \tag{1.101}$$

$$k^2 \left(\Phi + \Psi \right) = -8\pi G a^2 \sum_{\mathrm{a}} P_{\mathrm{a}} \Pi_{\mathrm{a}} \,, \tag{1.102}$$

$$\Psi - \Phi' = \frac{4\pi G a}{H} \sum_{\mathrm{a}} (\rho_{\mathrm{a}} + P_{\mathrm{a}}) \frac{\theta_{\mathrm{a}}}{k^2} \,, \tag{1.103}$$

$$\Psi' + \left(2 + 2\frac{H'}{H} - \frac{k_H^2}{3}\right)\Psi - \Phi'' - \left(2 + \frac{H'}{H}\right)\Phi' = \frac{4\pi G}{H^2}\left(\delta p + \frac{1}{3}\delta\rho\right) \quad (1.104)$$

where the sums run over all energy components. In the absence of anisotropic stresses both gravitational potentials are equal (up to a minus sign). At early times the difference in the two gravitational potentials is sourced by the second moment of the phase-space distribution function of radiation components. However at late times, well after decoupling and during the matter dominated phase, this is negligible and one can safely set $\Psi = -\Phi$ to obtain the standard growth of matter linear perturbations $\delta_m \propto a$. This is a key property of cold dark matter, allowing its perturbations to grow at the same rate for all scales well below the Hubble horizon during the matter dominated phase. At later times, once DE starts to become important, the growth of large scales structures is halted because the expansion becomes very fast and the pace of matter aggregation is reduced, even frozen for a de Sitter expansion. The details of how this process occurs depend on the very nature of DE. Matter components source the gravitational potential Φ through the Poisson equation, Eq. (1.101), however the trajectories of non-relativistic CDM particles respond to the gravitational potential Ψ through the geodesic equation, which in the Newtonian limit is $\ddot{\vec{x}} = -\nabla\Psi$. Hence, even if probes of the Universe's expansion indicate that DE should very close to a cosmological constant with $P \approx -\rho$, the growth of perturbations can be very different in the presence of the anisotropic stress Π_{de}. But note that this quantity is not accessible from background observations, and by taking a posture of complete ignorance about what DE is, it is natural to incorporate the stress in a perturbative analysis, on the same footing as one introduces the EoS and the speed of sound. The anisotropic stress should be small at early times, before decoupling, in order to not spoil the CMB anisotropies, tightly constraining models and leaving room to affect the CMB only through the ISW effect. Hence, it is expected that effects of a DE stress will be more feasible to be detected through CDM late time clustering probes, in particular the matter PS.

From the conservation of the energy-momentum tensor we get the continuity and Euler equations, for non-interacting fluids these reduce to

$$\delta\rho' + 3(\delta\rho + \delta P) = -(\rho + P)\left(3\Phi' + \frac{\theta}{aH}\right), \quad (1.105)$$

$$(\rho + P)\theta' = \frac{k^2}{aH}\big(\Psi(\rho + P) + \delta P\big) - (\rho' + P')\theta - 4(\rho + P)\theta - \frac{2}{3aH}k^2 P\Pi, \quad (1.106)$$

where we use derivatives with respect to $\ln(a)$, denoted by a prime. At the background level adiabaticity is guaranteed by the continuity equation, however, when

fluctuations are considered, the energy density of components and their EoS do not completely specify their pressure. In a general description, for non-interacting components one has the relation [67, 68, 13]:

$$\delta P = c_s^2 \delta\rho + 3aH(\rho + P)(c_s^2 - c_a^2)\frac{\theta}{k^2}, \tag{1.107}$$

with c_a the adiabatic sound speed and c_s the speed of sound in the fluid's rest frame,

$$c_a^2 \equiv \frac{P'}{\rho'}, \quad c_s^2 \equiv \frac{\delta P^{rest}}{\delta\rho^{rest}}, \tag{1.108}$$

where

$$\delta\rho^{rest} = \delta\rho + 3Ha(\rho + P)\frac{\theta}{k^2} \tag{1.109}$$

the last expression is the gauge invariant rest-frame density perturbation [65].

1.2.4 Matter comoving gauge

An alternative gauge choice is defined by choosing the components of the generator vector field, V^S_{com} and V_t^{com}, to obtain the metric conditions:

$$B = V_T \quad \text{and} \qquad \mathrm{H_T} = 0\,, \tag{1.110}$$

where V_T is the sum of velocities of matter components, excluding dark energy, this choice gives the solutions,

$$V^S_{com} = -a^2\tilde{H}_T, \quad V_t^{com} = a(V_T - \tilde{B}) + a^2\dot{\tilde{H}}_T\,. \tag{1.111}$$

For this metric it is better to rename the metric components as[6]:

$$\zeta \equiv H_L\,, \quad \xi \equiv A\,. \tag{1.112}$$

The Einstein's field equations, in matter comoving gauge are:

$$\zeta + \frac{V_T}{k_H} = \frac{4\pi G a^2}{k^2}\sum_{\mathrm{a}}\left(\delta\rho_{\mathrm{a}}^{\mathrm{com}} + 3Ha(\rho_{\mathrm{a}} + P_{\mathrm{a}})\frac{\theta_{\mathrm{a}} - \theta_T}{k^2}\right)\,, \tag{1.113}$$

$$\xi + \zeta + aH\frac{\theta_T' + 2\theta_T}{k^2} = -8\pi G a^2\sum_{\mathrm{a}} P_{\mathrm{a}}\Pi_{\mathrm{a}}\,,\,, \tag{1.114}$$

[6]In other notations the comoving curvature perturbation is named as: $H_L = \mathcal{R}$.

$$\xi - \zeta' = \frac{4\pi G a}{H} \sum_{\rm a} (\rho_{\rm a} + P_{\rm a}) \frac{\theta_{\rm a} - \theta_T}{k^2} \,, \tag{1.115}$$

$$\zeta' + \left(2 + 2\frac{H'}{H} - \frac{k_H^2}{3}\right)\zeta - \frac{1}{3aH}(\theta'_T + \theta_T) - \xi'' - \left(2 + \frac{H'}{H}\right)\xi' = \frac{4\pi G}{H^2}\left(\delta p^{com} + \frac{1}{3}\delta\rho^{com}\right) \tag{1.116}$$

The right hand side of the third Einstein field equation (1.115) can be simplified to yield,

$$\zeta' = \xi - \frac{\theta_T}{aHk^2} - \frac{4\pi G a}{H}(\rho_{de} + P_{de})\frac{\theta_{de} - \theta_T}{k^2} \,, \tag{1.117}$$

the Navier–Stokes equations for total matter

$$\delta\rho'_T + 3(\delta\rho_T + \delta p_T) = -(\rho_T + P_T)(k_H V_T + 3\zeta'), \tag{1.118}$$

$$\delta P_T - \frac{2}{3}P_T\Pi_T + (\rho_T + P_T)\xi = 0 \Rightarrow \xi = -\frac{\delta P_T - \frac{2}{3}P_T\Pi_T}{\rho_T + P_T}, \tag{1.119}$$

replacing ξ from the last equation in Eq.(1.117) it is obtained a conservation law for the comoving curvature ζ:

$$\zeta' = -\frac{\delta P_T - \frac{2}{3}P_T\Pi_T}{\rho_T + P_T} - \frac{\theta_T}{aHk^2} - \frac{4\pi G a}{H}(\rho_{de} + P_{de})\frac{\theta_{de} - \theta_T}{k^2} \,, \tag{1.120}$$

on super horizon scales $k \ll aH$ the curvature perturbation is conserved, $\zeta' \to 0$. The relationships between comoving and conformal Newtonian gauge are obtained by replacing the solutions of the gauge generator of interest, for example, using Eq.(1.111) one can go from comoving variables to Newtonian ones following the transformation rules (1.83)-(1.91), the transformation between the two scalar metric fluctuations is given by:

$$\Psi = \xi + \partial_t V_t^{com} = \xi + aH(V_T + V'_T) \tag{1.121}$$

$$\Phi = \zeta + HV_t^{com} = \zeta + aHV_T \tag{1.122}$$

Chapter 2

ΛCDM extensions

As has been mentioned, the ΛCDM model is the simplest, successful cosmological model supported by observations. An important aspect of the cosmological observations is that we can classify them into two groups. In the first one the cosmological observations are used to test the background model by probing the expansion history, and, in the second, it is possible to test perturbations around the background using observations that probe the CMB anisotropies and the growth of structure. For the background, we use distances between galaxies, luminosity distances coming from supernovae Ia, diameter angular distances of BAO, etc. All these observations are considered standard candles or/and standard rulers, and, they don't need a perturbed description. On the other hand, for the perturbations, we use mainly the CMB temperature power spectra, and observations of the large-scale structure. The perturbed universe provides crucial tests and more tightly constraints on the model parameters that are complementary to those arising from the background, therefore they should be consistent.

To describe all the cosmological observations, the ΛCDM model assumes the existence of two yet directly undetected components: CDM and DE to explain the accelerated expansion of the present universe. However, we are not at present sure that DE behaves exactly as a constant, it can well be a function of the cosmic time, and also can have additional properties, such as anisotropic stress. In its more general way to understand it, it can be considered as a fundamental scalar field or alternatively as an exotic type of fluid or some modified gravity scheme. These last approaches are equivalent at first order perturbation level, when the appropriate physical conditions are imposed, as we will describe in next chapter. In this chapter, we follow the fluid approach motivated to provide with a phenomenological prescription of DE. We will next consider a family of models that phenomenologically describe DE, considering different time behaviors.

2.1 Parameterized dark energy

Beyond a cosmological constant, the accelerated expansion of the universe can be driven by a dynamical DE component whose EoS is commonly parametrized by a time dependent function,

$$P_{de} = w(z)\rho_{de}, \tag{2.1}$$

where the EoS parameter, $w(z)$, can be chosen with different purposes; as for example, it can mimic quintessence and phantom fields [69, 70]. In general, quintessence models and then EoS parameterizations $w(z)$ can be classified into two broad categories: thawing and freezing behaviors [71, 72]. In the first case the scalar field is

frozen at early times where the kinetic energy is negligible and $w \sim -1$, then $w(z)$ evolves generically as a monotonic, convex, decreasing function to reach asymptotically, at late times, some $w \geq -1$. In the second case, in freezing-tracker models, the scalar field rolls down to the minimum of its potential at the beginning of the Universe, but starts to slow down and stops when it comes to dominate the dynamics; in this case the $w(z)$ function is generically a monotonic, concave, increasing function at higher z which at late times tends to $w \sim -1$. Several DE parametrizations have been proposed in the literature, some seem to favor thawing models [73, 74], but Ref. [75] exhibits that freezing models fit better. This latter reference proposes a generalization of the CPL EoS [76, 77], called nCPL,

$$w(z) = w_0 + w_a \left(\frac{z}{1+z}\right)^n , \tag{2.2}$$

or, in terms of the scale factor

$$w(a) = w_0 + w_a \left(1 - a\right)^n , \tag{2.3}$$

such that $n = 1$ reduces to the standard CPL (suitable for thawing models) while for larger values of n it can produce freezing behavior. Since the goal is to understand how different EoS behaviors influence different cosmological observations such as SNIa, BAO, H_0, CMB anisotropies and the PS, especially in combination with DE anisotropic stress, we will consider the nCPL parametrization with $n = 1$ and $n = 7$, corresponding to thawing and freezing behaviors, respectively. We will also consider models with w constant. For any $n > 0$, the nCPL EoS parametrization is w_0 at $z = 0$ and goes to $w_0 + w_a$ at high redshifts. A requirement to achieve a thawing behavior is that the function should be decreasing as z grows and so w_a must be negative, and to get a freezing evolution w_a must be positive. Fig.2.1 exhibits those behaviors.

The density evolution is found substituting the parameterization $w(a)$ in the integral Eq.(1.12) that looks like:

$$\rho_i(a) = \rho_i^0 \exp\left[-3\int_1^a \frac{1 + w_i(\bar{a})}{\bar{a}} d\bar{a}\right] , \tag{2.4}$$

that for nCPL has the solutions

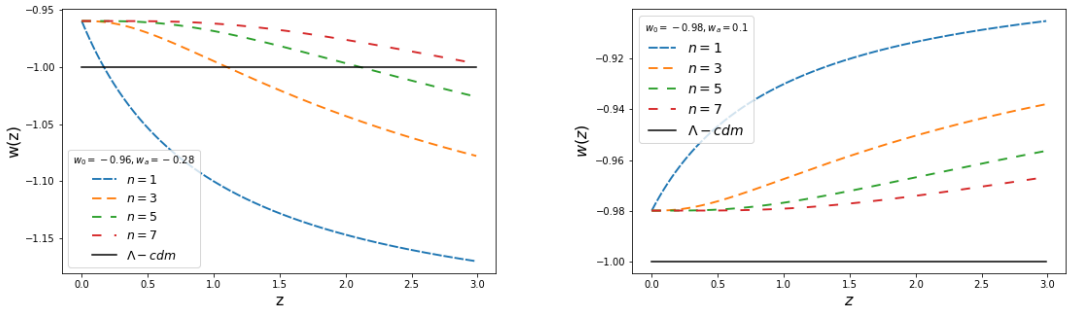

Figure 2.1: Left panel shows a decreasing $w(z)$ behavior, both parameters w_0, w_a are negative, and the convex behavior is guaranteed if $n = 1$ (thawing behavior). In the right panel $w_0 < 0$ but $w_a > 0$ in this case we obtain an increasing function, convex for $n > 1$(freezing).

$$\rho_{de}(a) = \begin{cases} \rho^0_{de} a^{-3(1+w_0+w_a)} \exp\left[-3w_a(1-a)\right] \quad (n=1), \\ \rho^0_{de} a^{-3(1+w_0+w_a)} \exp\left[-3w_a\left(\frac{363}{140} - 7a + \frac{21}{2}a^2 - \frac{35}{3}a^3 + \frac{35}{4}a^4 \right.\right. \\ \qquad \left.\left. -\frac{21}{5}a^5 + \frac{7}{6}a^6 - \frac{1}{7}a^7\right)\right] \quad (n=7)\,. \end{cases} \tag{2.5}$$

For parameter values $w_0 \neq -1$, $w_a \neq 0$ the DE density is not anymore constant on time as in the ΛCDM model and the new solution together with the other matter components determines the background history, $H(z)$, through the Friedmann equations Eq.(1.24).

2.2 Dark energy perturbations

One of the most powerful cosmological observations at first order perturbation level is the temperature map of the CMB, which contains a great deal of information: this map shows that there are small disturbances in the temperature distribution, called anisotropies. The observed CMB anisotropies could be originated before, during or after the LSS, by different sources, including the gravitational effect caused by the potential wells at recombination (the Sachs Wolfe effect, dominant on large angular scales), intrinsic temperature fluctuations at the time of the last scattering (dominant on small angular scales), and the Doppler effect from motions of the plasma. Since the time of LSS the photons of the CMB have been traveled through time varying potential wells, so, secondary anisotropies can be generated. Photons are blue shifted when they fall into a gravitational potential and redshifted when they climb out of it, if the potentials are decaying due to its linear evolution this effect is referred as the Integrated Sachs-Wolfe (ISW). A photon that crosses a varying potential well acquire a net energy shift, reflected in the CMB temperature map. During the matter dominated era, the gravitational potential is constant, (in the Newtonian gauge), which means that in that era there will not be any ISW effect produced. When dark energy starts to dominate over dark matter, the gravitational potentials are not constant anymore and the ISW term becomes significant, so this effect can be sourced by a time dependent DE density and its perturbations, reflected in the CMB map and its corresponding temperature power spectrum as shown in Fig.2.2.

In ΛCDM dark energy is a cosmological constant without density or pressure perturbations and without anisotropic stress, but if dark energy is modelled as a barotropic fluid with EoS parameter $w_0 \neq -1$ or by a depending time function $w(z)$, or by a scalar field, then small density and pressure fluctuations can be present at some specific epochs. The evolution of matter variables is given by the perturbed equations (1.105)-(1.109) which are valid for any barotropic fluid, in them it is necessary to specify the pressure equation. If w_i is just a positive constant, then, $P_i = w_i\rho_i$ implies that, both speed of sound definitions Eq.(1.108) coincide between them and with the w_i parameter and are well defined positive, explicitly;

$$\delta P_i = w_i \delta\rho_i \Rightarrow \frac{\delta P_i}{\delta\rho_i} \equiv c_{s,i}^2 = w_i\,, \quad \text{and} \qquad \dot{P}_i = w_i\dot{\rho}_i \Rightarrow \frac{\dot{P}_i}{\dot{\rho}_i} \equiv c_{a,i}^2 = w_i\,, \tag{2.6}$$

that happens for dark matter and radiation for example, however constant w dark energy models have negative values and so the speed of sound velocities can be also negative and different between them. The case when w_i is not a constant implies that temporal or spatial variations of w_i must be considered to specify the pressure

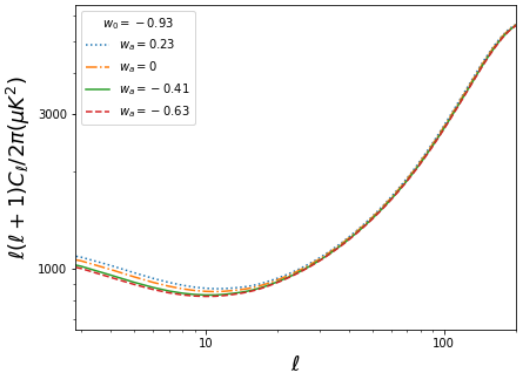

Figure 2.2: CMB temperature power spectrum at low ℓ-multipoles. In this plot the EoS of DE is the CPL parameterization. Here is explored the ISW effect that can be caused by changes on the w_0, w_a parameters. It was considered a fixed w_0 and different w_a values in the lack of DE anisotropic stress.

fluctuation Eq.(1.107):

$$\delta P_{de} = c^2_{s,de}\delta\rho_{de} + 3aH(1+w(z))\rho_{de}(c^2_{s,de} - c^2_{a,de})\frac{\theta_{de}}{k^2}, \tag{2.7}$$

$$c^2_a = w(z) - \frac{w'(z)}{3(1+w(z))}\,. \tag{2.8}$$

Check that if $w(z) = -1$ the equation (2.8) diverges. In this and following chapters DE is a fluid where $w(z)$ deviates from a cosmological constant and its density perturbation needs to be solved along with the Einstein equations.

$$\delta\rho'_{de} + 3(\delta\rho_{de} + \delta P_{de}) = -(\rho_{de} + P_{de})\left(3\Phi' + \frac{\theta_{de}}{aH}\right), \tag{2.9}$$

$$\begin{aligned}(1+w(z))\rho_{de}\theta'_{de} \;=\; & \frac{k^2}{aH}\big(\Psi(1+w(z))\rho_{de} + \delta P_{de}\big) - (\rho'_{de} + P'_{de})\theta_{de} \\ & -4(1+w(z))\rho_{de}\theta_{de} - \frac{2}{3aH}k^2 P_{de}\Pi_{de}\,.\end{aligned} \tag{2.10}$$

The anisotropic stress term also affects the shear equation, whose derivatives are involved in the ISW effect:

$$k^2\,(\Phi + \Psi) = -8\pi G a^2 P_{\rm T}\Pi_{\rm T} + P_{de}\Pi_{de}\,. \tag{2.11}$$

When $w(z)$ crosses the phantom divide ($w(z) = -1$) the velocity equation (2.10) becomes singular. There are different approaches to implement DE perturbations, specially to avoid the phantom divide, one of them is developed in the frame of gauge invariant entropy perturbation variables [67]; the relative entropy perturbation between the matter and the dark energy, and the intrinsic entropy perturbation of the dark energy. In terms of these entropy perturbations are rewritten and solved the Einstein's field equations. In this work DE perturbations are included using the PPF framework, this formalism has the advantage that allows to cross the phantom divide.

Chapter 3

PPF formalism

The parametrized post-Friedmann (PPF) formalism was initially proposed [44] to describe regimes where modified gravity (MG) models can accelerate the expansion of the Universe without dark energy. Any DE or MG model needs to guarantee an expansion history compatible with distance measures at large scales. Another requirement is that at linear regime it is obtained a modified Poisson equation, and on small scales modifications must be suppressed in order to satisfy stringent local tests of General Relativity (GR). To achieve all the cosmological requirements the PPF formalism introduces three functions, $g(a,k), f_\zeta, f_g$: the first one encodes the relationship between the two scalar metric fluctuations, the second for the super-horizon relationship between the metric and density fluctuations, and the third one to have the quasi–static limit in which the metric potential satisfies a Poisson–like equation. Additionally this formalism introduces one constant parameter, c_Γ, as the relationship between the transition scale and the Hubble scale.

What distinguishes a particular model of gravity or dark energy is the relationship between the metric potentials Φ and Ψ because they modify directly the shear equation (1.102). In the PPF framework a function g is introduced to establish a relationship between metric potentials:

$$g \equiv \frac{\Phi + \Psi}{\Phi - \Psi}\,, \tag{3.1}$$

g is related to the more commonly used slip parameter $\gamma \equiv -\Phi/\Psi$ as

$$g = \frac{\gamma - 1}{\gamma + 1}, \tag{3.2}$$

also it is useful to define the potentials Φ_-, Φ_+,

$$\Phi_- \equiv \frac{\Phi - \Psi}{2}, \quad \Phi_+ \equiv \frac{\Phi + \Psi}{2}\,. \tag{3.3}$$

Replacing the Einstein equations in Newtonian gauge it is obtained a Poison like equation for the potential Φ_-, that in the quasi–static regime, $k_H >> 1$ [1], when time derivatives of the metric fluctuations can be ignored compared with spatial gradients and the matter anisotropic stress is negligible yields,

$$k^2\Phi_- = \frac{4\pi G a^2}{1 + f_G}\delta\rho^{rest}\,, \tag{3.4}$$

here the $f_G(a)$ function is added to parameterize a possibly time-dependent modification of the Newton constant.

[1] ($k_H \equiv \frac{k}{aH}$)

Cosmological perturbations that give rise to the large scale structures in the universe (galaxies, clusters, etc) are assumed to be causally generated during the inflationary period by quantum fluctuations of the inflaton field. These primordial inhomogeneities grew bigger than the Hubble horizon (that coincides with the event horizon at that time) and due to exponential expansion then they exit it. After inflation the Hubble scale begins to grow more rapidly than the wavelength of perturbations and eventually the mode's wavelength re-enters the Hubble horizon as the perturbation seeds of structure formation [78].

The quasi–static approximation is not valid at all scales, and at superhorizon scales, $k_H << 1$, there can also be modifications that can be taken into account, with this purpose one can introduce an additional term Γ to the modified Poison equation,

$$k^2(\Phi_- + \Gamma) = 4\pi G a^2 \delta\rho^{rest} + P_T \Pi_T \,, \tag{3.5}$$

in this limit the derivative of the last equation along with the conservation equation gives an evolution equation for Γ that needs to be solved. Making a gauge transformation from Newtonian to comoving, and replacing the Φ_- definition it is obtained the next equation of motion for the curvature ζ,

$$\zeta' = (g+1)\Phi'_- + (1 - g + g')\Phi_- - aH'V_T \tag{3.6}$$

for which we have the freedom at superhorizon scales to determine the leading order behavior of ζ'. Without loss of generality, we can parametrize it with a possibly time-dependent function f_ζ, such that Eq.(1.117) is

$$\lim_{k_H<<1} \zeta' = -\frac{\delta P_T - \frac{2}{3} P_T \Pi_T}{\rho_T + P_T} + \frac{1}{3} f_\zeta k_H V_T \,. \tag{3.7}$$

Those are all the functions required by this framework, to demand all the requirements of GR. It sometimes uses variables in comoving gauge and then make the gauge transformation to Newtonian as was previous done. Particular choices of functions g, f_G, f_ζ are related to different MG models [44], and it is possible to extend this framework to DE models where DE anisotropic stress can modify the relationship between potentials and must be considered.

3.1 PPF for dark energy

There are different approaches to implement the evolution of DE anisotropic stress to solve the system 1.101-1.106. Some works [23, 24, 27, 28, 31, 33, 79] assume that anisotropic stress is sourced by the amplitude of the velocity shear tensor $\partial^i v^j_{de}$, and are motivated by the fact that it should be gauge invariant; so they demand to fulfill a continuity-like equation stemming from a Boltzmann hierarchy, but invoking an effective viscosity parameter as a source. This approach washes out DE fluctuations for non-phantom EoS [29], making them even more difficult to detect when compared to other approaches, as those motivated by MG [32] or modified growth [20], where effects inside the horizon are also expected. Both approaches are valid and are motivated by different physics. The specific model will then determine the effects on observables. Our motivation is to explore effects on scales that will be available through the next generation of LSS measurements.

First of all if DE is modelled by a fluid with a barotropic time dependent EoS and anisotropic stress is not negligible the continuity and Euler equations have the known expressions:

$$\delta\rho'_{de} = -3(\delta\rho_{de} + \delta P_{de}) - (\rho_{de} + P_{de})\left[k_H v_{de} + 3\Phi'\right] , \tag{3.8}$$

$$\frac{[a^4(\rho_{de} + p_{de})(v_{de})]'}{a^4 k_H} = \delta p_{de} - \frac{2}{3} p_{de}\Pi_{de} + (\rho_{de} + p_{de})\Psi, \tag{3.9}$$

it is useful to make the derivative of the last equation,

$$\frac{4a^3 a'}{a^4 k_H}(\rho_{de} + p_{de})v_{de} + \frac{a^4}{a^4}\frac{[(\rho_{de} + P_{de})(v_{de})]'}{k_H} = \delta P_{de} - \frac{2}{3} P_{de}\Pi_{de} + (\rho_{de} + P_{de})\Psi, \tag{3.10}$$

to finally obtain an expression that will be appear in next calculations,

$$\frac{[(\rho_{de} + p_{de})(v_{de})]'}{k} = \frac{\delta p_{de}}{aH} - \frac{2}{3}\frac{p_{de}\Pi_{de}}{aH} + \frac{(\rho_{de} + p_{de})\Psi}{aH} - 4(\rho_{de} + p_{de})\frac{v_{de}}{k}. \tag{3.11}$$

In ΛCDM the right hand side of Eq.(1.102) has only contributions coming from anisotropic stresses of neutrinos and radiation, but now, the potential Φ_+ is modified by the contribution of DE anisotropic stress,

$$\Phi_+ = -\frac{8\pi G a^2}{2}\frac{P_T\Pi_T}{k^2} - \frac{8\pi G a^2}{2}\frac{p_{de}\Pi_{de}}{k^2}, \tag{3.12}$$

in the PPF framework this deviation is parametrized by the $g(a, k)$ function,

$$\Phi_+ \equiv g(a, k)\Phi_- - \frac{4\pi G a^2}{k^2} P_T\Pi_T \, , \tag{3.13}$$

such that the metric ratio function has the definition,

$$g(a,k) = -\frac{4\pi G a^2 P_{de}\Pi_{de}}{k^2\Phi_-}, \tag{3.14}$$

check that if there is not DE anisotropic stress then $g = 0$ and Φ_+ has only the standard contributions, equation (3.14) replaces the DE anisotropic stress and its derivatives in terms of the PPF–function g and the potential Φ_-,

$$-\frac{4\pi G a^2 P_{de}\Pi_{de}}{k^2} = g\Phi_-, \tag{3.15}$$

taking the prime ($'$) derivative of the last expression it is obtained the derivative of the DE anisotropic stress in the new variables

$$\begin{aligned} -\frac{8\pi G a a' P_{de}\Pi_{de}}{k^2} - \frac{4\pi G a^2}{k^2}\left(P_{de}\Pi_{de}\right)' = g'\Phi_- + g\Phi_-' \Rightarrow \\ \frac{4\pi G a^2}{k^2}\left(P_{de}\Pi_{de}\right)' = 2g\Phi_- - g'\Phi_- - g\Phi_-' \,. \end{aligned} \tag{3.16}$$

The goal is to obtain a modified Poisson equation for the Φ_- potential, starting from it's definition:

$$k^2\Phi_- \equiv \frac{k^2\Phi}{2} - \frac{k^2\Psi}{2} = k^2\Phi - \frac{k^2\Phi}{2} - \frac{k^2\Psi}{2} = k^2\Phi - k^2\Phi_+ \,. \tag{3.17}$$

Replacing the Einstein equations (1.101) and (1.102) in the last equation yields,

$$k^2\Phi_- = 4\pi G a^2\left[\delta\rho_T^{rest} + \delta\rho_{de}^{rest}\right] + \frac{4\pi G a^2}{k^2}P_{de}\Pi_{de} + \frac{4\pi G a^2}{k^2}P_T\Pi_T \,, \tag{3.18}$$

the PPF formalism introduces a new function Γ, which encodes the no standard terms to this Poisson equation, for dark energy it takes the definition:

$$\Gamma = -\frac{4\pi G a^2}{k^2}\left[\delta\rho_{de}^{rest} + P_{de}\Pi_{de}\right] \,, \tag{3.19}$$

check that if there is not DE anisotropic stress Γ is not necessarily zero, because DE density perturbations are present, but if $\Gamma = 0$ the standard Poisson equation is recovered and there are not modifications comming from dark energy. The variable Γ allows to obtain a Poisson equation for an effective potential $\Phi_- + \Gamma$ sourced only by standard contributions,

$$k^2\left(\Phi_- + \Gamma\right) = 4\pi G a^2\left[\delta\rho_T^{rest} + P_T\Pi_T\right] \,, \tag{3.20}$$

One of the advantages of this framework is that solving the motion equation for Γ it is possible to recover the behavior of the dark energy variables, the motion equation for Γ is obtained deriving it's definition and replacing the conservation equations as follows,

$$\Gamma' = -\frac{8\pi G}{k^2}aa'\left[\delta\rho_{de} + 3aH(\rho_{de}+P_{de})\frac{V_{de}}{k} + P_{de}\Pi_{de}\right] - \frac{4\pi Ga^2}{k^2}\Big[\delta\rho'_{de} + 3a'H(\rho_{de}+P_{de})\frac{V_{de}}{k} + 3aH'(\rho_{de}+P_{de})\frac{V_{de}}{k} + 3aH\left[(\rho_{de}+P_{de})\frac{V_{de}}{k}\right]' + (P_{de}\Pi_{de})'\Big], \tag{3.21}$$

replacing again the Γ definition, the equation for H' and the conservation equations, Eqs. (3.8), (3.11),

$$\begin{aligned}\Gamma' = 2\Gamma &- \frac{4\pi Ga^2}{k^2}(P_{de}\Pi_{de})' - \frac{4\pi Ga^2}{k^2}\Big[-3\delta\rho_{de} - 3\delta P_{de} - (\rho_{de}+p_{de})\frac{kV_{de}}{aH} \\ &- 3(\rho_{de}+p_{de})\Phi'\Big] - \frac{4\pi Ga^2}{k^2}\left[3aH(\rho_{de}+p_{de})\frac{V_{de}}{k}\right] \\ &- \frac{4\pi Ga^2}{k^2}3(\rho_{de}+p_{de})\frac{V_{de}}{k}a\left[-\frac{4\pi G}{H}(\rho_T + P_T + \rho_{de} + P_{de})\right] \\ &- \frac{4\pi Ga^2}{k^2}3aH\left[\frac{\delta P_{de}}{aH} - \frac{2}{3}\frac{P_{de}\Pi_{de}}{aH} + \frac{(\rho_{de}+P_{de})\Psi}{aH} - 4(\rho_{de}+P_{de})\frac{V_{de}}{k}\right],\end{aligned} \tag{3.22}$$

reordering terms,

$$\begin{aligned}\Gamma' = 2\Gamma &- \frac{4\pi Ga^2}{k^2}(P_{de}\Pi_{de})' - \frac{4\pi Ga^2}{k^2}\Big[-3\delta\rho_{de} - 9aH(\rho_{de}+P_{de})\frac{V_{de}}{k} - 2P_{de}\Pi_{de} \\ &- P_{de}\Pi_{de}\Big] - \frac{4\pi Ga^2}{k^2}P_{de}\Pi_{de} - \frac{4\pi Ga^2}{k^2}\left[3\Psi - 3\Phi'\right] + \frac{4\pi Ga^2}{k^2}(\rho_{de}+P_{de})\frac{kV_{de}}{aH} \\ &- \frac{4\pi Ga^2}{k^2}3(\rho_{de}+P_{de})\frac{V_{de}}{k}\left[-\frac{4\pi Ga}{H}(\rho_T + P_T + \rho_{de} + P_{de})\right].\end{aligned} \tag{3.23}$$

Replacing the Einstein equation (1.103) it is obtained,

$$\begin{aligned}\Gamma' = 2\Gamma - 3\Gamma &- \frac{4\pi Ga^2}{k^2}P_{de}\Pi_{de} - \frac{4\pi Ga^2}{k^2}(P_{de}\Pi_{de})' \\ &- \frac{4\pi Ga^2}{k^2}(\rho_{de}+P_{de})12\pi G\frac{a}{H}\left[(\rho_T+P_T)\frac{V_T}{k} + (\rho_{de}+P_{de})\frac{V_{de}}{k}\right] \\ &+ \frac{4\pi Ga^2}{k^2}(\rho_{de}+P_{de})\frac{kV_{de}}{aH} - \frac{4\pi Ga^2}{k^2}(\rho_{de}+P_{de})3\frac{V_{de}}{k}\left[-\frac{4\pi Ga}{H}(\rho_T + P_T + \rho_{de} + P_{de})\right].\end{aligned} \tag{3.24}$$

Reordering terms in the last expression and replacing the anisotropic stress contributions in terms of PPF variable using Eqs. (3.15) and (3.16),

$$\Gamma' = -g\Phi_- + g'\Phi_- + g\Phi'_- - \frac{4\pi G a^2}{k^2}\left[12\pi G\frac{a}{H}(\rho_{de}+P_{de})\left(\frac{V_T}{k}-\frac{V_{de}}{k}\right)\right](\rho_T+P_T) + \frac{4\pi G a^2}{k^2}(\rho_{de}+P_{de})\frac{kV_{de}}{aH} - \Gamma \tag{3.25}$$

The previous equation is written in mostly PPF variables, excepting for the concerning terms to DE velocity, this DE contribution appears also in the motion equation of the curvature ζ' Eq.(1.117) for which the extra contributions are parametrized at large scales, $k_H \ll 1$, by a depending time function f_ζ;

$$\lim_{k_H\ll 1} 4\pi G\frac{a}{H}(\rho_{de}+P_{de})\left(\frac{V_{de}}{k}-\frac{V_T}{k}\right) = -\frac{1}{3}f_\zeta\frac{k}{aH}V_T \tag{3.26}$$

in this superhorizon limit the equation of motion for Γ is :

$$\lim_{k_H\ll 1}\Gamma' = -\Gamma - g\Phi_- + g'\Phi_- + g\Phi'_- + \frac{4\pi G a^2}{k^2}(\rho_T+P_T)\left(-f_\zeta k_H V_T\right) + \frac{4\pi G a^2}{k^2}(\rho_{de}+P_{de})k_H V_T\,. \tag{3.27}$$

The term Φ'_- can be expressed in terms of PPF functions, it's expression is found by deriving Eq.(3.20),

$$\Phi_- = \frac{4\pi G a^2}{k^2}\left[\delta\rho_T + 3aH(\rho_T + P_T\frac{V_T}{k}) + P_T\Pi_T\right] - \Gamma\,, \tag{3.28}$$

with respect $'$,

$$\Phi'_- = -\Gamma' + \frac{8\pi G a a'}{k^2}\left[\delta\rho_T + 3aH(\rho_T+P_T)\frac{V_T}{k} + P_T\Pi_T\right] + \frac{4\pi G a^2}{k^2}\Big[\delta\rho'_T + 3aH'(\rho_T+P_T\frac{V_T}{k}) + 3a'H(\rho_T+P_T)\frac{V_T}{k} + 3aH\left((\rho_T+P_T)\frac{V_T}{k}\right)' + (P_T\Pi_T)'\Big]\,, \tag{3.29}$$

replacing the continuity and Euler equations for the matter component in Eq.(3.29)

yields,

$$\begin{aligned}\Phi'_- = 2\Phi_- + 2\Gamma - \Gamma' + \frac{4\pi G a^2}{k^2}\Big[&- (\rho_T + P_T)(k_H V_T + 3\Phi') - 3(\delta\rho_T + \delta P_T) \\ &+ 3aH(\rho_T + P_T)\frac{V_T}{k} + 3a(\rho_T + P_T)\frac{V_T}{k}\frac{4\pi G}{3H}(\rho'_T + \rho'_{de}) + 3aH\frac{k_H}{k}\delta P_T \\ &+ 3aH\frac{k_H}{k}(\rho_T + P_T)\Psi - 2P_T\Pi_T - 12aH(\rho_T + P_T)\frac{V_T}{k} + (P_T\Pi_T)'\Big] \end{aligned} \tag{3.30}$$

reordering terms in last expression and then replacing the terms Φ_- and Γ where it is required,

$$\begin{aligned}&\Phi'_- = 2\Phi_- + 2\Gamma - \Gamma' + \frac{4\pi G a^2}{k^2}\left[-3\delta\rho_T - 9aH(\rho_T + P_T)\frac{V_T}{k} - 3P_T\Pi_T\right] + \frac{4\pi G a^2}{k^2}\left[P_T\Pi_T\right. \\ &\left.+(P_T\Pi_T)' - (\rho_T + P_T)(k_H V_T + 3\Phi') + 3a(\rho_T + P_T)\frac{V_T}{k}\frac{4\pi G}{3H}(\rho'_T + \rho'_{de}) + 3(\rho_T + P_T)\Psi\right] \\ &= 2\Phi_- + 2\Gamma - \Gamma' - 3(\Phi_- + \Gamma) + \frac{4\pi G a^2}{k^2}\left[P_T\Pi_T + (P_T\Pi_T)'\right] + \frac{4\pi G a^2}{k^2}3(\rho_T + P_T)\left[\Psi - \Phi'\right] \\ &+ \frac{4\pi G a^2}{k^2}\left[-(\rho_T + P_T)k_H V_T + (\rho_T + P_T)\frac{V_T}{k}\frac{a}{H}(-12\pi G)(\rho_t + P_T + \rho_{de} + P_{de})\right] \end{aligned} \tag{3.31}$$

$$\begin{aligned}&= -\Phi_- - \Gamma - \Gamma' + \frac{12\pi G a^2}{k^2}(\rho_T + P_T)\left[4\pi G\frac{a}{H}(\rho_T + P_T)\frac{V_T}{k} + 4\pi G\frac{a}{H}(\rho_{de} + P_{de})\frac{V_{de}}{k}\right] \\ &- \frac{12\pi G a^2}{k^2}(\rho_T + P_T)\left[4\pi G\frac{a}{H}(\rho_T + P_T)\frac{V_T}{k} + 4\pi G\frac{a}{H}(\rho_{de} + P_{de})\frac{V_T}{k}\right] \\ &- \frac{4\pi G a^2}{k^2}(\rho_T + P_T)k_H V_T + \frac{4\pi G a^2}{k^2}\left[P_T\Pi_T + (P_T\Pi_T)'\right]. \end{aligned} \tag{3.32}$$

Finally, Φ'_- has the motion equation:

$$\begin{aligned}\Phi'_- \;=\; &-\Phi_- - \Gamma - \Gamma' + \frac{12\pi G a^2}{k^2}(\rho_T + P_T)4\pi G\frac{a}{H}(\rho_{de} + P_{de})\left(\frac{V_{de} - V_T}{k}\right) \\ &-\frac{4\pi G a^2}{k^2}(\rho_T + P_T)k_H V_T + \frac{4\pi G a^2}{k^2}\left[P_T\Pi_T + (P_T\Pi_T)'\right] \end{aligned} \tag{3.33}$$

The last equation is valid at all scales, because it hasn't been considered any limit, however considering the parametrization Eq.(3.26) to replace the remaining DE con-

tribution at superhorizon scales $k_H \ll 1$ yields,

$$\begin{aligned}\lim_{k_H\ll 1}\Phi'_- &= -\Phi_- - \Gamma - \Gamma' + \frac{12\pi G a^2}{k^2}(\rho_T + P_T)\left[-\frac{1}{3}f_\zeta(a)\frac{k}{aH}V_T\right] \\ &\quad -\frac{4\pi G a^2}{k^2}(\rho_T + P_T)k_H V_T + \frac{4\pi G a^2}{k^2}\left[P_T\Pi_T + (P_T\Pi_T)'\right], \quad (3.34)\end{aligned}$$

and regrouping terms it is obtained the motion equation of Φ_- in this limit:

$$\lim_{k_H\ll 1}\Phi'_- = -\Phi_- - \Gamma - \Gamma' - \frac{4\pi G a^2}{k^2}(\rho_T + P_T)\left[f_\zeta + 1\right]k_H V_T + \frac{4\pi G a^2}{k^2}\left[P_T\Pi_T + (P_T\Pi_T)'\right], \quad (3.35)$$

substituting equation (3.35) in the expression for Γ' (3.27):

$$\begin{aligned}&\lim_{k_H\ll 1}\Gamma' = -\Gamma - g\Phi_- + g'\Phi_- - g\Phi_- - g\Gamma - g\Gamma' - \frac{4\pi G a^2}{k^2}(\rho_T + P_T)\left[gf_\zeta + g\right]k_H V_T \\ &+ g\frac{4\pi G a^2}{k^2}\left[P_T\Pi_T + (P_T\Pi_T)'\right] - \frac{4\pi G a^2}{k^2}(\rho_T + P_T)f_\zeta k_H V_T + \frac{4\pi G a^2}{k^2}(\rho_{de} + P_{de})f_\zeta k_H V_T \quad (3.36)\end{aligned}$$

reducing terms:

$$\begin{aligned}\lim_{k_H\ll 1}\Gamma'(1+g) &= -\Gamma(1+g) + (g' - 2g)\Phi_- + g\frac{4\pi G a^2}{k^2}\left[P_T\Pi_T + (P_T\Pi_T)'\right] \\ &\quad -\frac{4\pi G a^2}{k^2}\left[(\rho_T + P_T)\left[gf_\zeta + g + f_\zeta\right] - (\rho_{de} + P_{de})\right]k_H V_T\,, \quad (3.37)\end{aligned}$$

defining the source of the last equation:

$$\begin{aligned}S &= \frac{4\pi G a^2}{(1+g)k^2}\left(g\left[P_T\Pi_T + (P_T\Pi_T)'\right] - \left\{(\rho_T + P_T)\left[gf_\zeta + g + f_\zeta\right]\right.\right. \\ &\quad \left.\left.-(\rho_{de} + P_{de})\right\}k_H V_T\right) + \frac{(g' - 2g)}{(1+g)}\Phi_-\,, \quad (3.38)\end{aligned}$$

and now rewriting the equation of motion for Γ in the limit $\lim_{k_H\ll 1}$

$$\lim_{k_H\ll 1}\Gamma' = S - \Gamma\,. \quad (3.39)$$

Note that the source S vanishes if the functions g and f_ζ are zero, in this case there is not modification to gravity.

In the opposite limit, $k_H \gg 1$, the DE anisotropic stress should vanish and the potential Φ_- have also a Poisson equation with a possible modified Newton constant, introduced by the f_G PPF function:

$$\lim_{k_H \gg 1} \Phi_- = \frac{4\pi G a^2}{k^2} \frac{\delta\rho_T^{rest} + P_T \Pi_T}{1 + f_G(a)} \,, \tag{3.40}$$

a comparison between (3.40) and (3.20) implies that in the quasistatic regime

$$\lim_{k_H \gg 1} \Gamma = f_G \Phi_- \,. \tag{3.41}$$

The equation of motion for Γ [45, 25] must be valid at all scales. To satisfy the super horizon limit $k_H \ll 1$ and the subhorizon scales $k_H \gg 1$ the equation of motion for Γ is taken to be:

$$\left(1 + c_\Gamma^2 k_H^2\right) \left[\Gamma' + \Gamma + c_\Gamma^2 k_H^2 (\Gamma - f_G \Phi_-)\right] = S \,, \tag{3.42}$$

where c_Γ is a new PPF parameter. Those are all the required equations for the PPF prescription, where giving the functions $g(a,k)$, f_ζ and f_G. It is possible to solve for Γ and after recover the dark energy variables. For example, the rest frame density perturbation, δ_{de}^{rest} is obtained from Eq.(3.19), then, using equation (3.15) to substitute the anisotropic stress in terms of g, after we use eq. (3.20) to eliminate Φ_-, and finally regrouping terms,

$$\begin{aligned}
\frac{4\pi G a^2}{k^2} \left[\delta\rho_{de}^{rest}\right] &= -\Gamma - \frac{4\pi G a^2}{k^2} P_{de} \Pi_{de} \,, \\
\frac{4\pi G a^2}{k^2} \left[\delta\rho_{de}^{rest}\right] &= -\Gamma + g\Phi_- \,, \\
4\pi G a^2 \left[\delta\rho_{de}^{rest}\right] &= -(g+1)k^2\Gamma + g\left[4\pi G a^2 \delta\rho_T^{rest}\right] \,.
\end{aligned} \tag{3.43}$$

This formalism also allow us to across the phantom divide. The numerical implementation to solve the system has been done in CAMB [63] and CosmoMC [80, 81] and the main results for different dark energy parametrizations are detailed in the following subsection.

3.1.1 Dark energy stress phenomenology

To solve the perturbed equations in the PPF formalism the functions; $f_\zeta(a), f_G(a)$, $g(a,k)$ and the constants c_s^2, c_Γ must be specified. We know that dark energy becomes important and not negligible at large scales, this is the limit $k_H \ll 1$, where we can

expect $g(a,k) \neq 0$ and at least $\mathcal{O}(k_H^{-2})$, also we expect $\Gamma \neq 0$. In the opposite limit we want to restore general relativity, because of that we will fix $f_G = 0$. We need to construct an appropriated g function to obtain deviations when it are required.

The function $g(a,k)$ used in this work has the following functional form [25]:

$$g(a,k) = \frac{g_{SH}(a)}{1 + (c_g k_H)^2}\,, \tag{3.44}$$

also we know that the role of dark energy starts to be important at late times when it becomes to dominate over dark matter, at background level the ratio between densities varies along a, this motivates the functional form of g_{SH}:

$$g_{SH}(a) = g_0 \left(\frac{\rho_{de}(a)}{\rho_m(a)} \frac{\Omega_m^0}{\Omega_{de}^0} \right)^{1/2}\,. \tag{3.45}$$

This $g(a,k)$ function introduces two additional free parameters, g_0 and c_g, its amplitude and propagation along k-modes, respectively. For $g_0 = 0$ one recovers the case without anisotropic stress and $c_g = 0$ implies scale free dependence. These functions affect the Poisson equation (1.101), which using equations(3.19), hop (3.15) can be rewritten in terms of g as

$$k^2 \Phi_- = \frac{4\pi G a^2 (\delta\rho_m^{rest} + \delta\rho_{de}^{rest})}{1+g}\,, \tag{3.46}$$

from this we can see that $g > 0$ makes Φ_- to diminish, as was shown in [25]. Also it is possible to express Eq.(3.46) in terms of DE anisotropic stress and matter perturbations:

$$P_{de}\Pi_{de} = -\frac{g}{1+g}\left[\delta\rho_T^{rest} + \delta\rho_{de}^{rest}\right]. \tag{3.47}$$

By construction in this formalism DE anisotropic stress has contributions of all energy density perturbations and the different components are weighted by the same factor as Eq.(3.47) indicates. Other approaches that include DE anisotropic stress [32, 82] parameterize the right hand side of Eq. (3.47) using different weight factors to each matter perturbation.

Chapter 4

Cosmological effects of DE anisotropic stress.

In this chapter we present the main results of this thesis. We employ the equations of previous chapters to incorporate anisotropic stress of DE, and although it was motivated by MG models, its parameterization is suitable as a fluid description to treat it in a phenomenological manner.

The results of this chapter use the PPF formalism to include DE anisotropic stress, with functions and parameters as follows: $f_G = 0$, $g(a,k)$ given by equation (3.44), $f_\zeta = 0.4\, g_{SH}$, $c_\Gamma = 0.4\, c_s^2$, and $c_s^2 = 1$, following ref. [25]. Varying the DE sound speed (c_s) it is known to provoke variations of up 2% in the matter power spectrum [16], but we set it constant here to concentrate our analysis in the anisotropic stress. To close the system it is necessary to specify the anisotropic stress parameters (g_0, c_g), that are in the function $g(a,k)$.

The DE contribution was numerically solved by adapting the codes `CAMB`[1] [63] and `CosmoMC`[2] [80] to include the shear contribution as detailed in the previous sections. We analyze the outcomes of the above anisotropic stress phenomenological model in combination with the effects of different DE EoS. The cosmological data set used in this work is: BAO measurements from 6dFGS, SDSS-MGS, and BOSS LOWZ BAO [55, 56, 57, 58], supernovae from the Combined Pantheon Sample [51], recent H_0 measurement from Riess 2018 [49], CMB TT spectrum and low-ℓ polarization data from Planck 2015 [3]. The main results are separated considering first the case without and with DE anisotropic stress and different DE EoS parametrizations that are detailed in the upcoming subsections.

4.1 No DE anisotropic stress

The results of these subsections consider that DE density perturbations are caused only by the EoS parametrization and $\Pi_{de} = 0$, then the ppf function $g(a,k) = 0$.

4.1.1 $w_{de}-$ constant

The case where the EoS parameter is just a constant, $w(z) = w_0 \neq -1$, guarantees an accelerated expansion of the universe if w_0 is smaller than $-1/3$.

There are two important regions, the non phantom with EoS parameter values, $-1 < w_0 < -1/3$, and the phantom region with $w_0 < -1$. First to explore similarities and differences between those regions they are explored separately. The results for

[1] https://camb.info/https://camb.info/

[2] https://cosmologist.info/cosmomc/https://cosmologist.info/cosmomc/.

non phantom region shows density perturbations well defined positive and different from zero for small k–modes. Fig.4.1 shows the results of the density contrast in its rest frame for different w_0 and c_s^2 values and allows to check that lower speed of sound values produce bigger DE density perturbations, and also that if w_0 is further away from a cosmological constant then the perturbations are further away from zero. For the phantom region, $w_0 < -1$, the perturbations can be also different

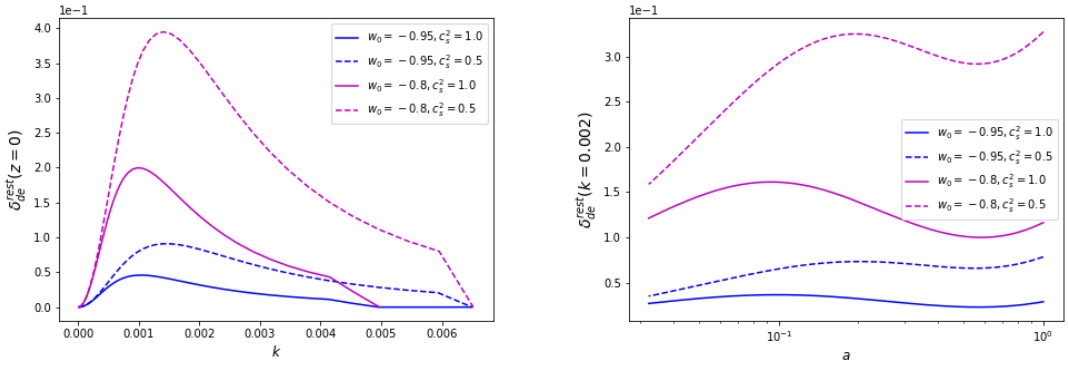

Figure 4.1: Dark energy perturbations with EoS $w_0 > -1$, non-phantom region, left plot fixes $z = 0$ and shows the dark energy perturbation for different k-modes, right plot sets a k mode and evolves it over the scale factor a.

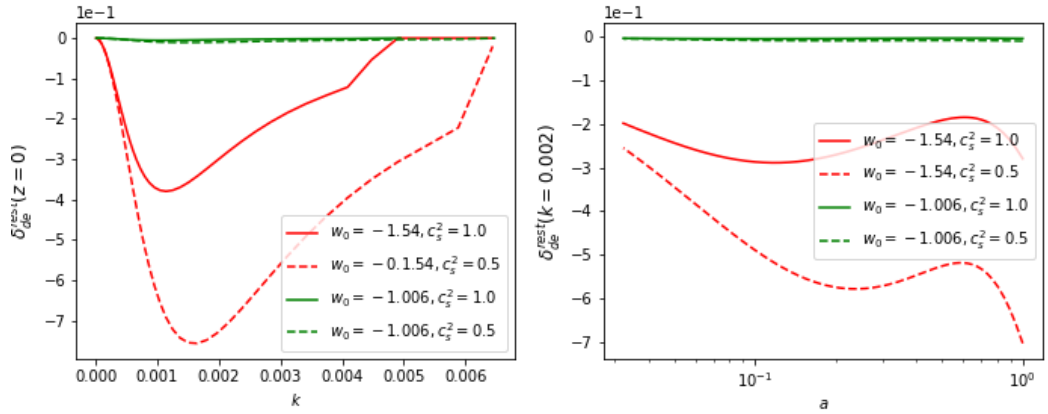

Figure 4.2: Phantom region, $w_0 < -1$, left panel fixes $z = 0$ and shows the dark energy density perturbation for different k-modes, right plot sets a k mode and evolves it over a.

from zero and negative as shown in Fig.4.2, where the chosen w_0 values are -1.54 and -1.006. The value $w_0 = -1.54$ is the best fit reported by Planck 2015 [3] when only CMB data are taken into account and $w_0 = -1.006$ is the result when also background observations are considered; updates of the CMB data yields similar constraints on this parameter. In this region also while w_0 deviates more from a cosmological constant its perturbations are further away from zero, and the effect of c_s^2 is the same than previously.

DE density perturbations are smaller than the matter ones, as shown in Figs. 4.3- 4.4 where it is plotted the ratio between dark energy and matter perturbations. This relation tends to zero in both regions. Fig. 4.5 shows the effect of different w_0

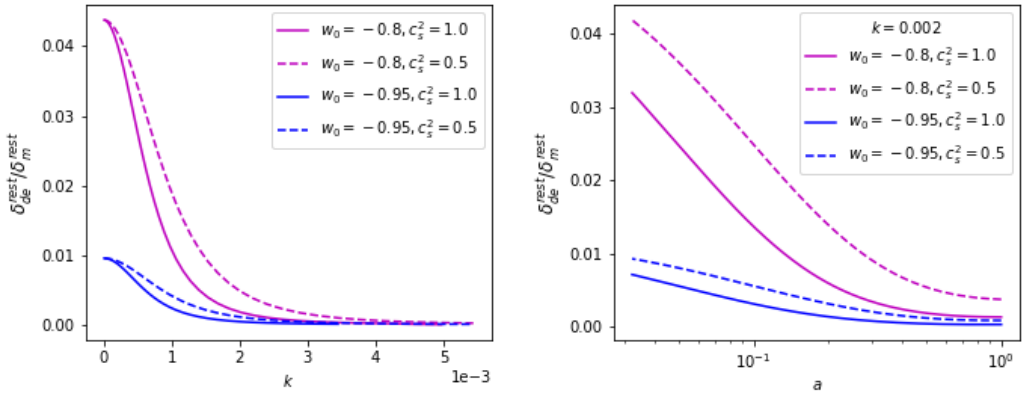

Figure 4.3: Non phantom region, $w_0 > -1$, these plots show the ratio between contrast densities. Left plot fixes $z = 0$, and the right panel sets a k mode and evolves it over a.

values on the CMB temperature power spectrum at low ℓ-multipoles.

4.1.2 Thawing- Freezing parametrizations.

The nCPL parametrization (2.2) has a thawing behaviour if $n = 1$, $w_0 < 0$ and $w_a < 0$, and a freezing behaviour if $n = 7$, $w_0 < 0$ and $w_a > 0$. Both behaviors can or not cross the phantom divide, if they don't across this barrier they remain in the phantom or non phantom region all the time.

The first election of EoS parameters,$w_0 = -0.86$, $w_a = -0.13$, gives a decreasing $w(z)$ function, which has a thawing behavior if $n = 1$, Fig. 4.6 shows the DE perturbations for different n and c_s^2 values. The second election is $w_0 = -0.98, w_a =$

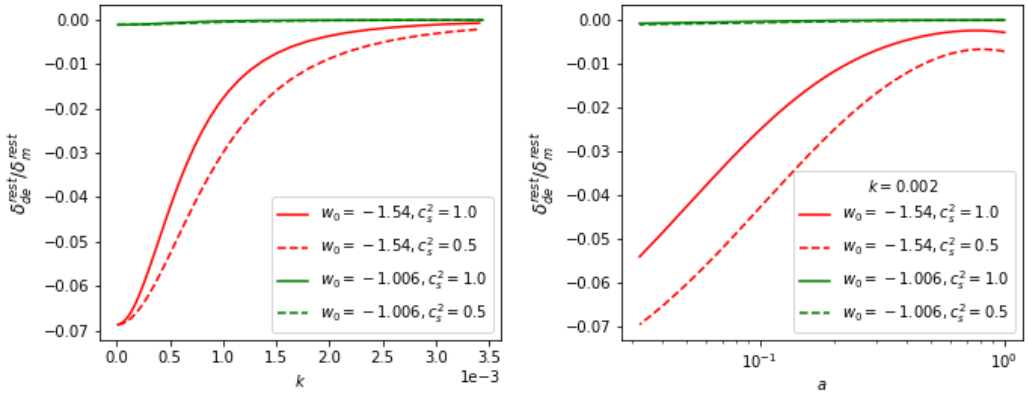

Figure 4.4: $w_0 < -1$ phantom region, these plots show the relation between contrast densities. Left plot fixes $z = 0$ for different k-modes, right plot sets a k mode and evolves it over a.

0.1, in this case the freezing behavior is obtained if $n = 7$, otherwise $w(z)$ is only an increasing function and the effect of n and c_s^2 is similar to the previous cases.

Almost all data sets from cosmological probes are compatible with phantom dark energy, in that case $w_0 + w_a$ can be less than -1, for this example $w_0 = -0.961, w_a = -0.28$ which are in agreement with Planck 2018. Plot 4.8 shows that the effect of n and c_s^2 is the same as in previous case: in this case perturbations are positive in the same regime where $w(z)$ is positive.

4.2 DE anisotropic stress

4.2.1 $w \approx -1$

DE emulating a cosmological constant at background level has no density perturbations in the absence of DE anisotropic stress. However, one expects that evolving DE will have differences, albeit small, from $w = -1$. But, for all practical purposes many DE/MG models are indistinguishable from ΛCDM at background level, so for definiteness we adopt $w = -1$ in this subsection. The inclusion of anisotropic stress generates fluctuations that depend on the chosen anisotropic stress parameters: bigger g_0 values generate bigger perturbation amplitudes; and, bigger c_g values shift the anisotropic shear effects to larger scales. These behaviors are shown in

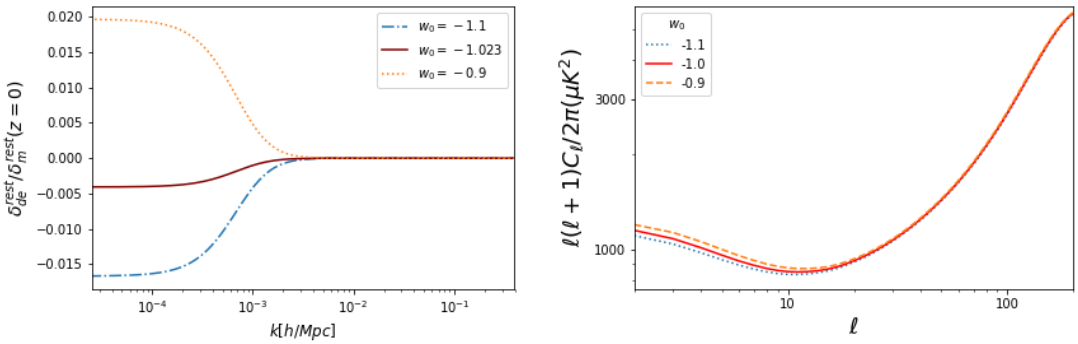

Figure 4.5: DE density contrast (left panel), CMB temperature power spectrum at low ℓ-multipoles (right panel) for different w_0 in which we neglected DE anisotropic stress.

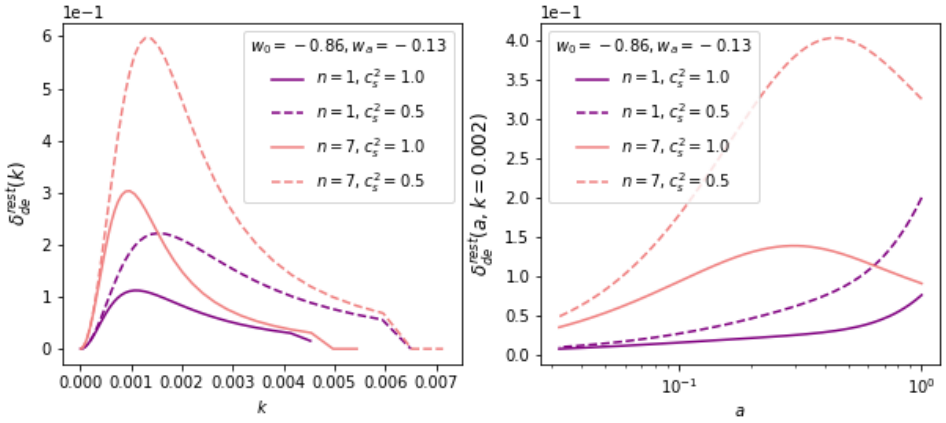

Figure 4.6: Dark energy contrast density for the nCPL parametrization with thawing behaviour if $n = 1$, for this w_0, w_a values, the power $n = 7$ is only a decreasing parametrization but is not thawing or freezing.

Fig. 4.9, where ratios of DE to matter rest-frame densities are plotted for parameters $g_0 = 0.18, 0.32$ and $c_g = 0.01, 0.1$. These values are chosen because they lie inside the 1-σ and 2-σ confidence interval levels (c.l.) allowed by the Monte Carlo Makov Chain (MCMC) (as we will show in Fig. 4.15), and still provide large deviations to the matter PS, reaching a maximum of 15% when compared to the ΛCDM ($g_0 = 0$) case, as explained below.

We varied the parameters (g_0, c_g) using `CAMB` to obtain various CMB TT power

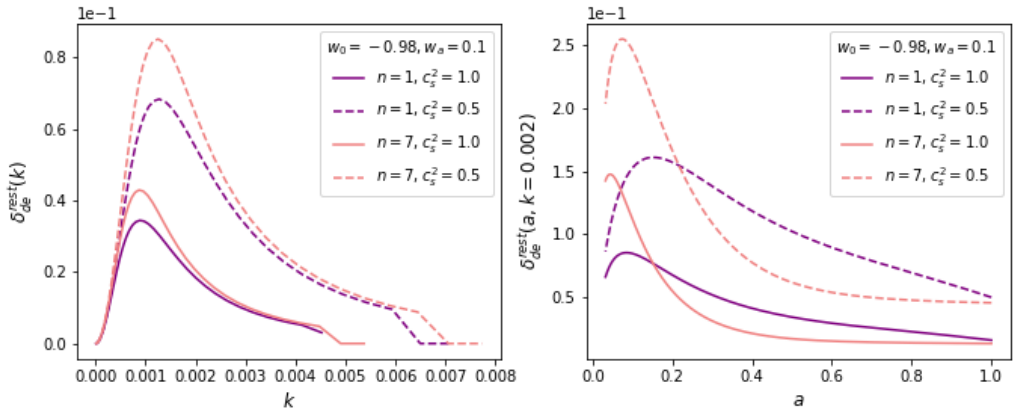

Figure 4.7: Contrast DE density perturbation with w_0, w_a parameters that yields a freezing behaviour if $n = 7$.

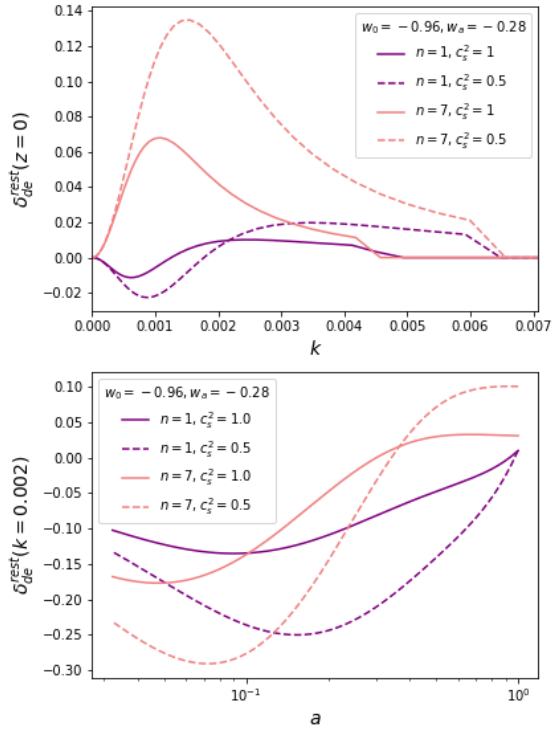

Figure 4.8: Contrast DE density perturbation with different EoS parameters.

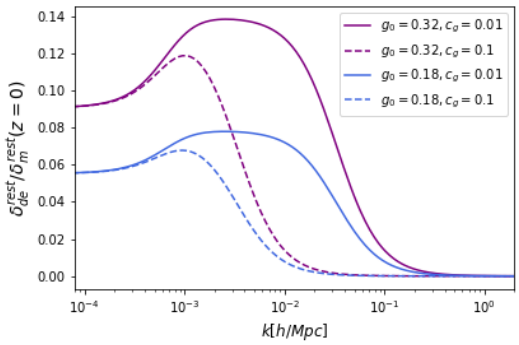

Figure 4.9: Ratios of DE to DM rest-frame densities at redshift $z = 0$. We employ an EoS with $w_0 = -1$ and various anisotropic stress parameters (g_0, c_g).

spectra, as shown in Figs. 4.10-4.11 along with CMB Planck data [3]. Left panel of Fig.4.10 has c_g fixed and shows that positive g_0 values enhance low-ℓ anisotropies due to the ISW, whereas negative values diminish them, except for very low multipoles, where multipoles can go crossing the ΛCDM curve to overtake it. We also show the

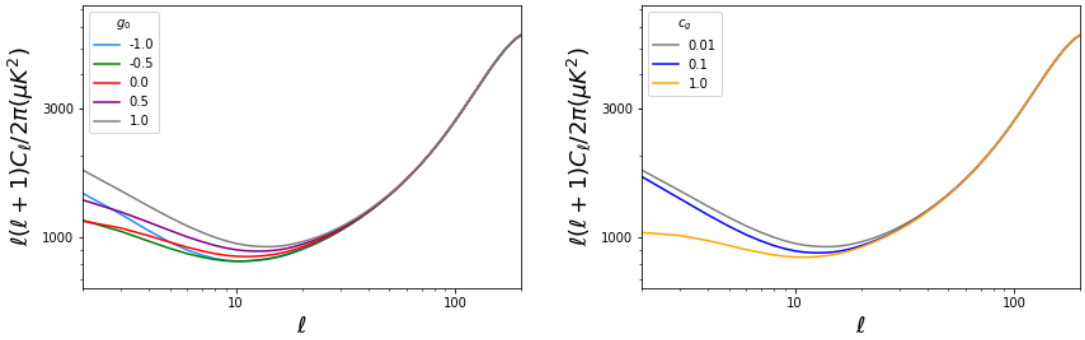

Figure 4.10: CMB TT power spectra at low multipoles for different g_0 (top panel, fixed $c_g = 0.01$) and c_g values (bottom panel, fixed $g_0 = 1.0$), for the $w = -1$ model.

ΛCDM best fit (black dashed line), labeled in the figure as $g_0 = 0, c_g = 0$. We note in the right panel of Fig. 4.10 that setting g_0 fixed, the effect of increasing c_g is both to decrease the low-ℓ anisotropies and to shift their effect to smaller ℓ-modes. These plots exhibits that, as we expected, the anisotropic parameters are not affecting high ℓ-multipoles, where all the plotted curves coincide. For low-multipoles anisotropies, one may try to adjust downwards the curve, however, the relevance of these data

points lies in the cosmic variance. In fact, low multipoles, including the quadrupole, turn out to be consistent with the ΛCDM model [83].

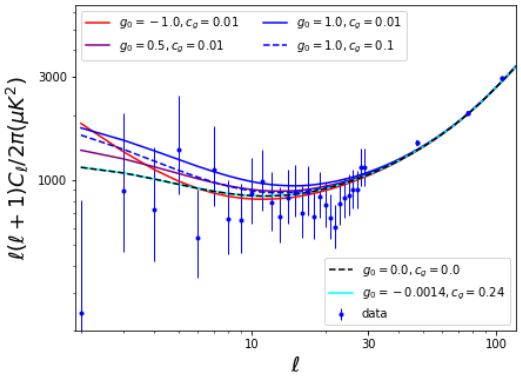

Figure 4.11: CMB TT power spectra at low multipoles for different c_g and g_0 values and EoS $w_0 = -1$. The best fit values are $g_0 = -0.0014, c_g = 0.24$, as shown in Table 4.1.

Large scale anisotropic stress imprints an effect on the clustering of matter at late times, as in the PS and growth function [23, 24, 29, 30, 31, 32, 33]. To see this, we plot the PS in Fig. 4.12 for (g_0, c_g) parameter values such that c_g is fixed and g_0 takes values between $[-1, 1]$, in a similar way we did it in Fig. 4.10. The effects over this matter statistic are clear: negative values of g_0 tend to rise the PS for low k-modes, and for large k we recover the ΛCDM model since $g(k \to 0) \to 0$; positive g_0 values produce the opposite effect. Note that we have fixed the normalization such that all models have the same primordial power spectrum amplitude A_s and spectral index n_s. For that reason all models coincide for modes $k_H \gg c_g^{-1}$, where g becomes negligible.

Now, selecting some of the parameters of Fig. 4.11, we show in Fig. 4.13 again the percentage departures with respect to the ΛCDM model: $c_g \to 0$ increases the effect. These deviations in the PS amplitude can be large in the range of linear perturbations, and in fact they will also contribute to the nonlinear PS [46].

We know, however, that deviations from the ΛCDM PS at scales ~ 0.01-$0.1\, h/\text{Mpc}$ could not be as large as in Fig. 4.12 or 4.13, since these would affect the BAO features, and given the upcoming galaxy surveys such as DESI [17], the constraints will tighten to uncertainties to be less than (or order of) 1%. Consequently, we explore for deviations that are of the order of 1% and at most 15% (up to an overall normalization) in Fig. 4.14, left and right panels, respectively. Note that the deviations from

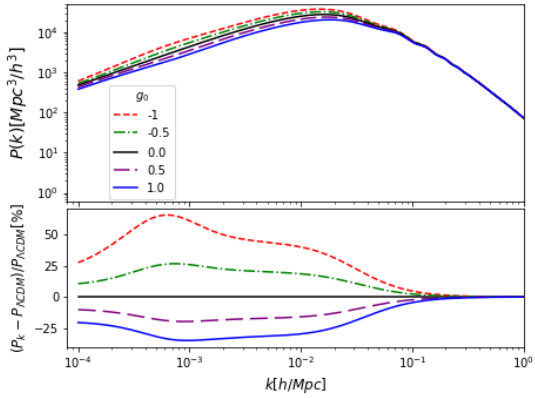

Figure 4.12: Matter PS produced by different g_0 values with $c_g = 0.01$ fixed. The bottom panel shows the percent differences with respect to ΛCDM model. The background model is $w_0 = -1$ EoS.

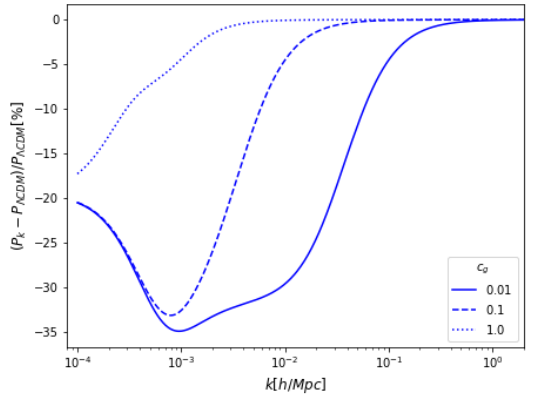

Figure 4.13: Percent deviations on the PS relative to the ΛCDM case produced by different c_g values with fixed $g_0 = 1$. The background model is $w_0 = -1$ EoS.

ΛCDM reach their maximum around $k \sim 10^{-3}\,h$/Mpc. At the scale $k \sim 0.01\,h$/Mpc, deviations are of 10% (left panel, models $g_0 = |0.32|$, $c_g = 0.01$) and of 0.66% (right panel, models $g_0 = |0.022|, c_g = 0.01$) and at $k \sim 0.05\,h$/Mpc of 4% (left panel) and of 0.3% (right panel).

In both panels of Fig. 4.14, dashed lines are for $c_g = 0.1$, solid lines for $c_g = 0.01$ and color changes for different g_0 as it is shown in the labels. Negative values of g will increase the potentials wells, as can be seen from Eq. (3.46), and then the PS

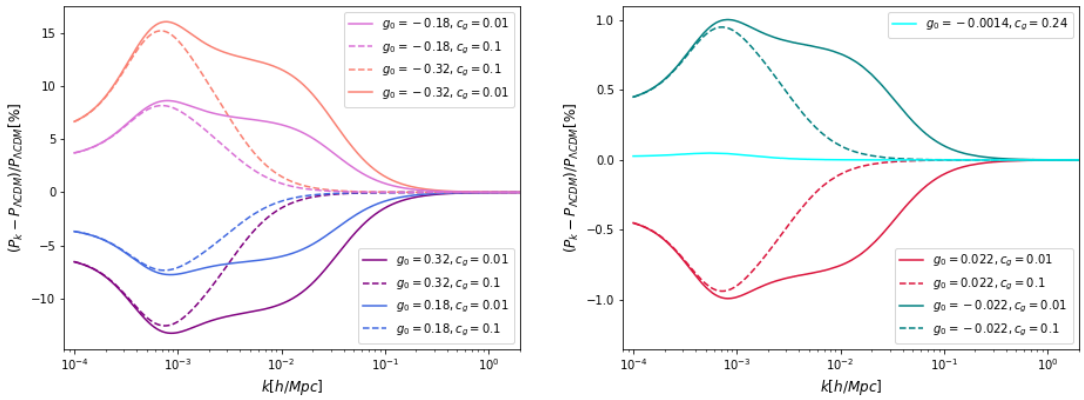

Figure 4.14: PS percentage deviation from ΛCDM. The anisotropic parameters (g_0, c_g) considered are such that the maximum percentage deviation is of around 15% (left panel) and of 1% (right panel), corresponding to 4.09% and to 0.28% at a scale $k = 0.05\,h/\text{Mpc}$, respectively. We include the best fitted plot of our data set (see the results table 4.1) corresponding to $g_0 = -0.0014, c_g = 0.24$ that produce a difference of around 0.05% from ΛCDM model. These results are for the $w_0 = -1$ EoS model.

increases as well. Increasing c_g lowers the absolute value of the maxima ($g_0 < 0$) or mimina ($g_0 > 0$), but this is a by-effect of the produced shift along k, that erases shear fluctuations above $k_H \sim c_g^{-1}$. Here we appreciate that deviations of at most 15% are possible if $|g_0| < 0.32$. In the right panel, we find g_0 values in the interval $|g_0| \leq 0.022$ permit at most order 1% deviations from the ΛCDM model.

To find out what anisotropic parameter values are more realistic and preferred by cosmological data we perform an MCMC sampling of the parameter space using `CosmoMC` and the cosmological data set described at the beginning of this section. The relevant best-fit values for the $w = -1$ model are in column I of Table 4.1. For anisotropic parameters we obtain $g_0 = -0.0014^{+0.1530}_{-0.1504}, c_g^2 < 0.070$ at 68% c.l., in agreement with the results of the vanilla ΛCDM cosmological parameters from Planck [3]. The CMB TT power spectrum produced by these values is included in Fig. 4.10 (cyan color) that is alike the ΛCDM model, meanwhile other models vary only at low-multipoles, as already explained. Similarly, in the right panel of Fig. 4.14, we include the PS of our best-fit to obtain deviations of around 0.05% at $k < 10^{-3}h/\text{Mpc}$ from the no anisotropic stress case.

We finalize this subsection presenting the contour confidence region of the stress parameters in Fig.4.15, and also the contour plots of the main cosmological parameters in Fig.4.16, confirming that the no-anisotropic case ($g_0 = 0$) is allowed at 1-σ

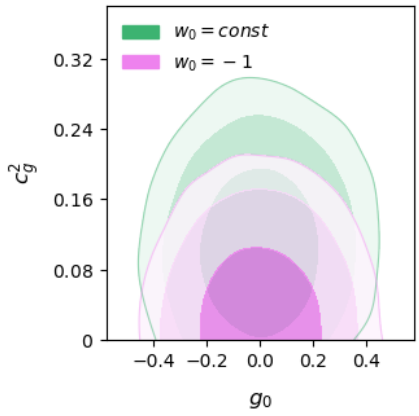

Figure 4.15: Contour confidence plots of the DE anisotropic parameters (g_0, c_g) at 68, 95 and 99% c.l. for the $w = -1$ and $w_0 =$ constant EoS models.

by CMB data. Nevertheless, the left panel of Fig. 4.14 shows that for anisotropic parameter values that are inside the 2-σ best-fit values, they produce differences on the PS of at least 15% with respect to ΛCDM. In this parameter range the CMB will be well fitted and not changing significantly. It is then clear that the PS imposes tighter constraints than the CMB on the anisotropic stress and hence is a potential theory discriminator of different DE anisotropic stress models.

4.2.2 $w =$ constant

In this section the expansion history is slightly different from ΛCDM, now we assume $w = w_0$ constant. Thus, density fluctuations are generated even if DE does not possess anisotropic stress, showing that perturbations attenuate as $w \to -1$ and when $c_s \to 1$.

For this model, anisotropic stress parameters leave very similar imprints on the CMB TT curve as those of the $w = -1$ model, see Fig. 4.10, so we omit to show these results, and the same discussion about the parameters (g_0, c_g) prevails for this EoS. The effects on the PS are shown in Fig.4.17, where the EoS reference value is $w_0 = -1.023$ in agreement with Planck's results [3] and the values c_g and g_0 were chosen so that they result in visible changes, with deviations from ΛCDM of order of 10% or less. For these plots we obtain a maximum deviation of around 10% at $k \sim 10^{-3}h$/Mpc, and of 3.4% at $k = 0.05h$/Mpc. All anisotropic stress values we used to generate Fig. 4.17 are consistent with the Planck CMB TT measurements.

The relevant results of an MCMC fit are presented in column II of Table 4.1, and

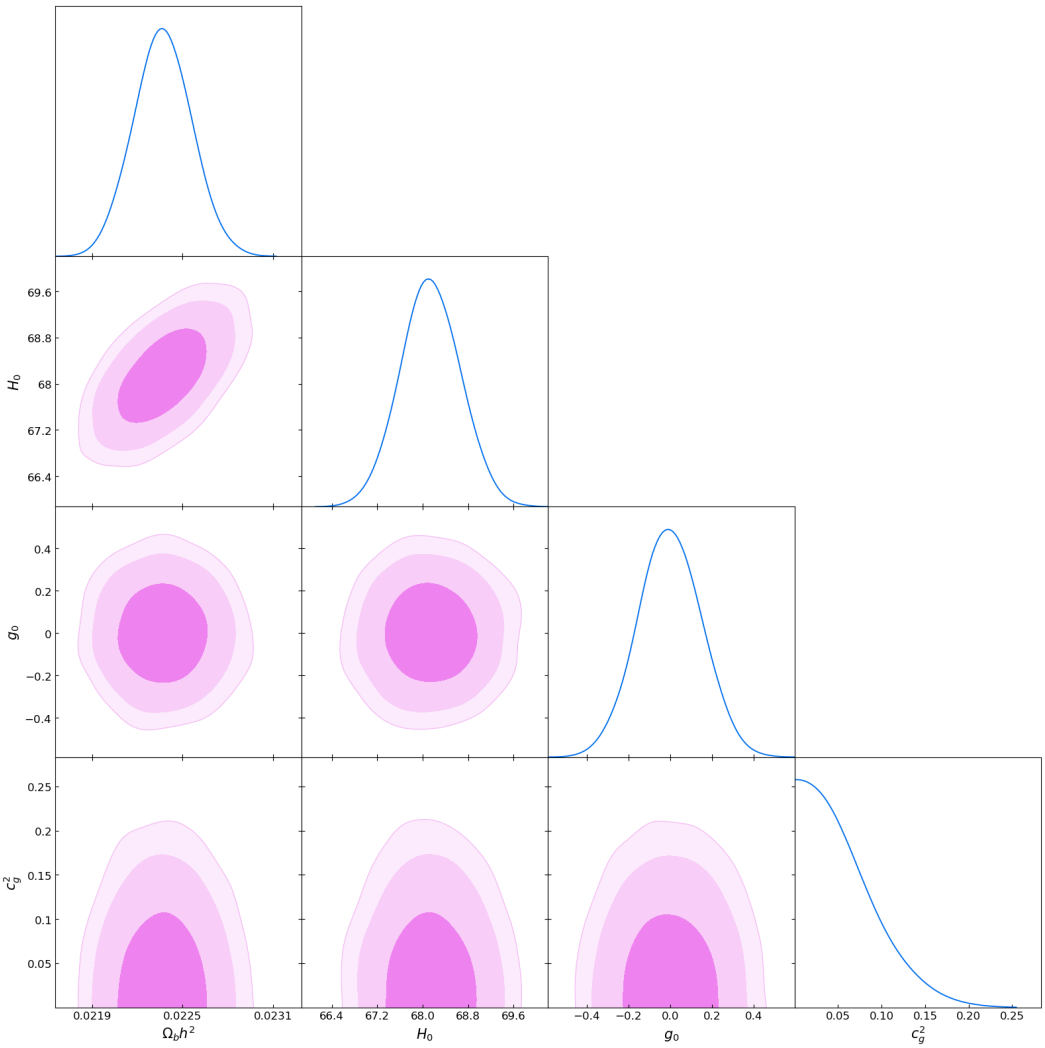

Figure 4.16: Contour confidence plots of the main cosmological parameters at 68, 95 and 99% c.l. for the $w = -1$ model.

Table 4.1: Best-fit values and marginalized 0.68 confidence intervals for our cosmological data set JLA, BAO, CMB TT and low-P. Column I corresponds to $w = -1$ EoS, in column II the parameter w_0 is a free constant, in column III the CPL parameterization with w_0, w_a as free parameters, in column IV the 7CPL parameterization with no anisotropic stress, and in column V the 7CPL parameterization with anisotropic stress.

	I $w = -1$	II w_0 constant	III CPL	IV 7 CPL no-stress	V 7 CPL
$\Omega_b h^2$	0.0224 ± 0.0002	0.0223 ± 0.0002	0.0222 ± 0.0002	0.0228 ± 0.0002	0.0223 ± 0.0002
$\Omega_c h^2$	0.1180 ± 0.0012	0.1191 ± 0.0016	0.1201 ± 0.0019	$0.1190^{+0.0017}_{-0.0016}$	0.1193 ± 0.0016
τ	$0.0855^{+0.0176}_{-0.0174}$	$0.0802^{+0.0184}_{-0.018}$	$0.0757^{+0.0189}_{-0.0188}$	$0.0795^{+0.0185}_{-0.0182}$	$0.0796^{+0.0183}_{-0.0186}$
$\log A_s$	$3.101^{+0.035}_{-0.034}$	3.093 ± 0.036	3.086 ± 0.036	3.090 ± 0.036	3.092 ± 0.036
n_s	0.970 ± 0.004	0.967 ± 0.005	0.965 ± 0.005	0.967 ± 0.005	0.967 ± 0.005
H_0	68.26 ± 0.53	68.99 ± 1.01	$68.83^{+1.02}_{-1.03}$	$68.97^{+1.00}_{-1.04}$	68.97 ± 1.00
w_0	-1.00	-1.046 ± 0.045	$-0.962^{+0.099}_{-0.111}$	-1.040 ± 0.047	$-1.040^{+0.046}_{-0.047}$
w_a	0	0	$-0.381^{+0.469}_{-0.352}$	< 0.882	< 0.873
g_0	$-0.0014^{+0.1530}_{-0.1504}$	$-0.0014^{+0.1531}_{-0.1539}$	$0.0004^{+0.1515}_{-0.1502}$	0	$0.0001^{+0.1510}_{-0.1520}$
c_g^2	< 0.070	$0.109^{+0.052}_{-0.069}$	< 0.071	0	< 0.071

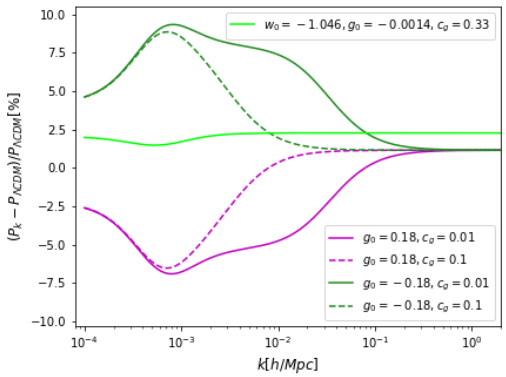

Figure 4.17: PS percentage deviation with respect ΛCDM. In these plots $w_0 = -1.023$, and g_0, c_g are as the labels indicate; we include the best-fit curve from Table 4.1.

the contour plots that involve DE parameters are shown in Figs. 4.15 and 4.18. The resulting parameter g_0 is similar to the one produced by the $w_0 = -1$ EoS, but c_g^2 has some differences, since now the intervals at 68, 95 and 99% are a slightly bigger and $c_g^2 = 0$ is excluded at 1-σ. As expected, the values $w_0 = -1, g_0 = 0$ are inside the 68% contours, and $c_g^2 = 0$ at 2-σ, meaning that the results are in agreement with the ΛCDM model.

Finally, we note that the value of c_g reported in Table 4.1 is bigger than for the other models. This motivated us to show in Fig. 4.18 the contour plots of the anisotropic parameters with the EoS parameter to clarify any degeneracy among them. We found essentially no degeneracy in w_0 and g_o, and a small effect in w_0 and c_g, as also proved in their corresponding correlation matrices in a principal component analysis. In Fig.4.19 there are shown the contour confidence plots of the main cosmological parameters.

4.2.3 Thawing parametrization (CPL)

Now we consider the CPL EoS, providing a thawing behavior for $w_a < 0$. CPL is one of the most popular EoS for DE, and according to Planck 2015 results [3] in the absence of DE anisotropic stress, the best fit values for the data set we are using are $w_0 = -0.93^{+0.23}_{-0.22}$, $w_a = -0.41^{+0.87}_{-0.91}$ at 2-σ [84], that we will take as reference values.

We found similar effects due to the anisotropic parameters on the CMB TT power spectrum for this EoS. We plot in Fig. 4.20 our results on deviations of the PS with

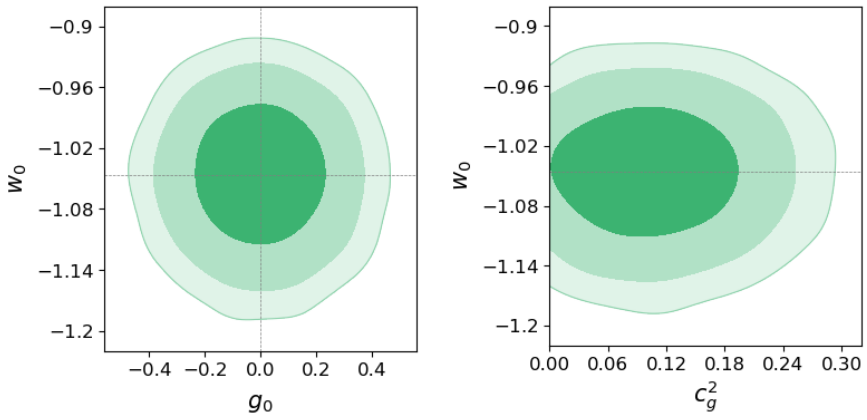

Figure 4.18: Contour confidence plots at 68, 95 and 99% for the w_0 =constant EoS, corresponding to results in column II of Table 4.1.

respect to ΛCDM model, as in Fig. 4.14 (left panel) and Fig.4.17, yielding maximum differences of around 10%; particularly, at $k = 0.05\,h/\text{Mpc}$ the maximum deviation is about 4%.

Finally, we performed an MCMC statistical analysis parametrizing w_{de} as CPL. The best-fit parameters and c.l. at 68% are presented in column III of Table 4.1, and their corresponding contour plots for (g_0, c_g) in Fig. 4.21. The contour plot for anisotropic stress parameters looks very similar to the one obtained with the EoS $w_0 = -1$; see Fig. 4.15, which indicates that the DE EoS and stress parameters are quite independent, this also is evident from Fig.4.22 where are shown the contour limits of the main cosmological parameters.

4.2.4 Freezing parametrization (7-CPL)

Finally we consider the n-CPL DE parametrization, Eq. (2.2) with $n = 7$ which has a freezing behavior if $w_0 < 0$ and $w_a > 0$. To our knowledge, for this EoS there are no reported best-fitted values for w_0, w_a. Then, we first estimate them for the case of null anisotropic stress. The results are shown in column IV of Table 4.1 and the contour plot is presented in Fig.4.23 (yellow regions). For this EoS the standard cosmological model is recovered ($w_0 = -1$, $w_a = 0$) at 68%. The w_0 parameter is well restricted by late time observations, whereas w_a is not sensitive to these cosmological data set, its upper limit at 68% is 0.882 but it can take a wide range of negative values. This is consistent with claims in the sense that fittings suggest thawing [73, 74] and freezing models [75]; we find that both are allowed for

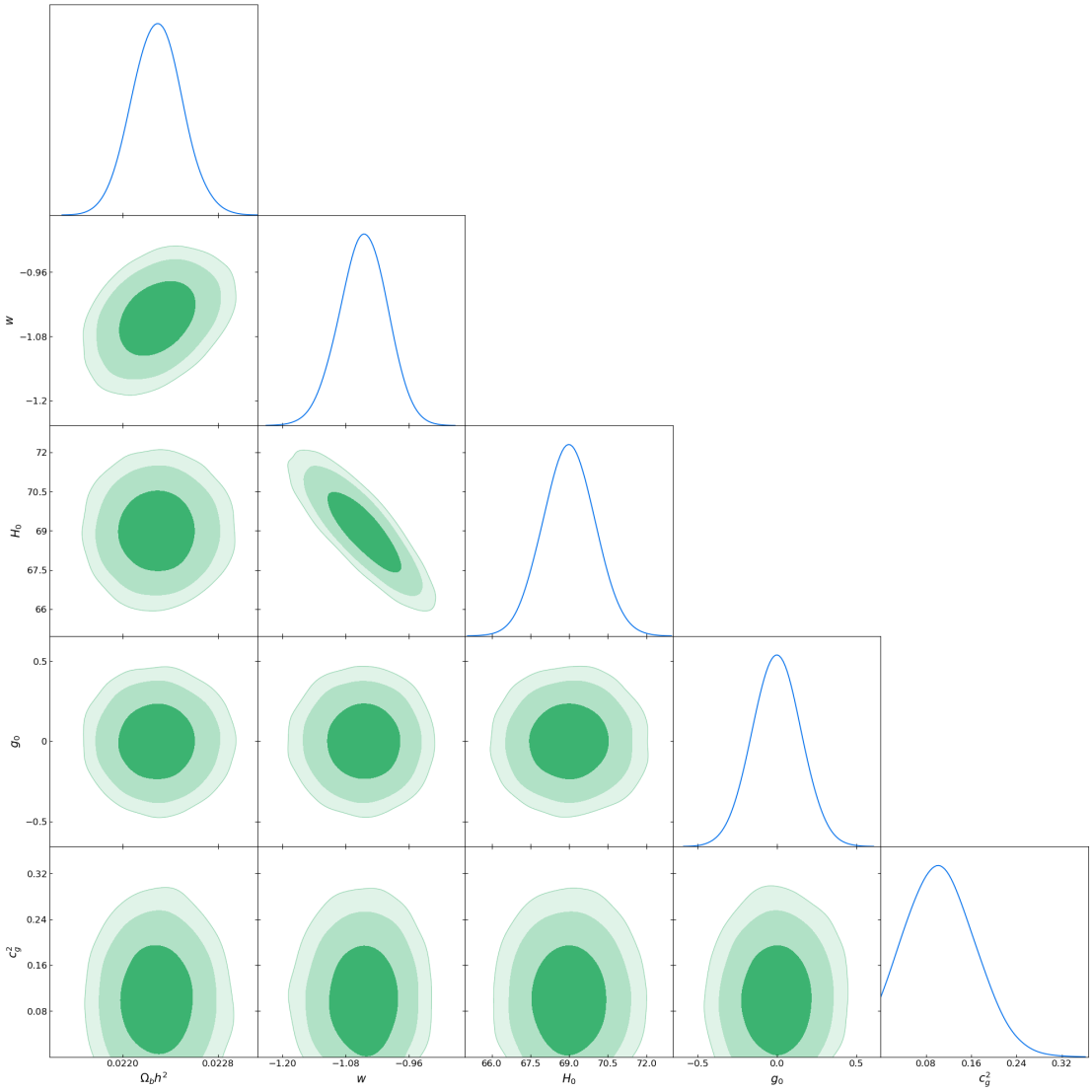

Figure 4.19: Contour confidence plots of the main cosmological parameters at 68, 95 and 99% c.l. for the $w = \text{const}$ model.

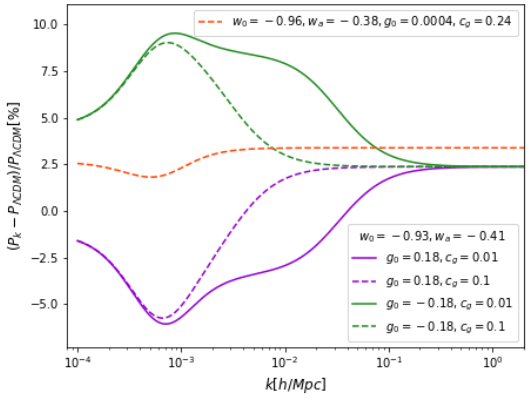

Figure 4.20: Deviations on the PS, produced by CPL parameterization and DE anisotropic stress. The parameters of DE EoS are $w_0 = -0.93$, $w_a = -0.41$, that are the Planck's reference values. We also include our best DE fitted parameters, shown in column III of Table 4.1.

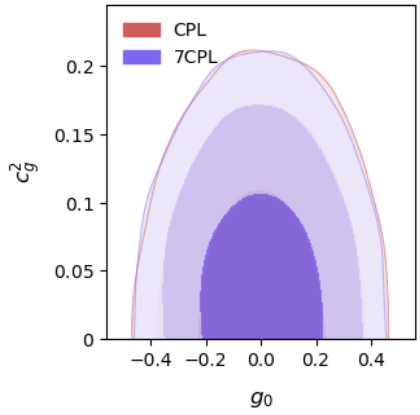

Figure 4.21: Contour confidence plots at 68, 95, and 99% of the parameters (g_0, c_g) for models CPL and 7CPL.

this EoS. Variations on w_a are not visible in the CMB TT, but deviations are present in the amplitude of the matter PS. When varying w_a from -1.1 to 0.8 the change in the PS is of about 1% in linear scales and these tend to lower the power, the larger (positive) w_a values are. In this case, the effects in the PS occur in k between 10^{-4} and 10^{-3} h/Mpc; after $k = 0.004\,h$/Mpc the PS behaves as ΛCDM.

Now we introduce DE anisotropic stress as in the above subsections. The data fits

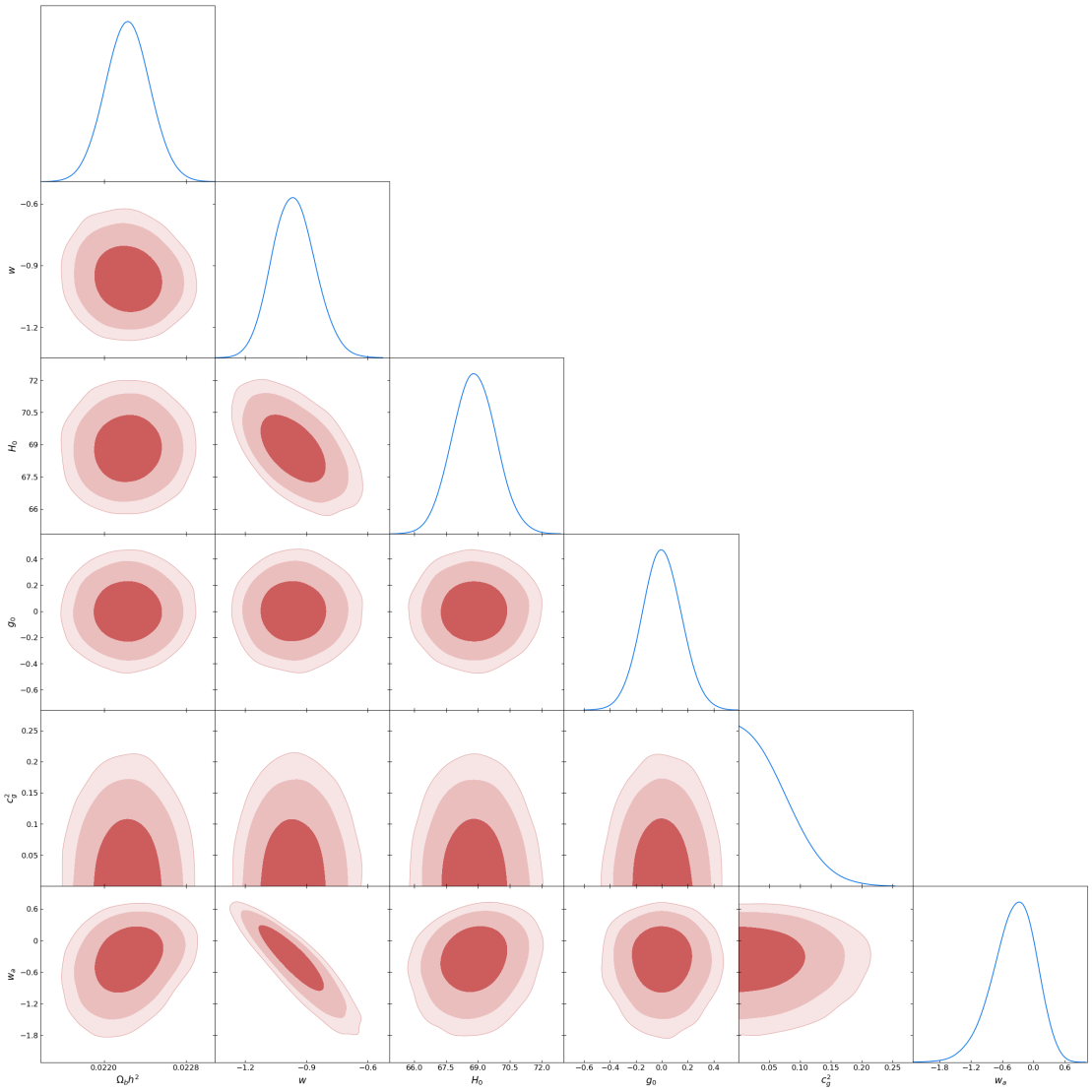

Figure 4.22: Contour confidence plots of the main cosmological parameters at 68, 95 and 99% c.l. for the CPL parameterization.

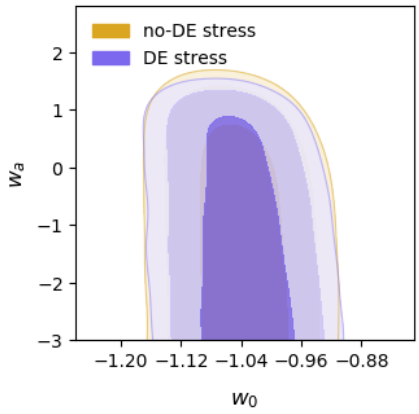

Figure 4.23: Contour confidence plots at 68, 95, and 99% for 7CPL EoS parameters with and without DE anisotropic stress.

are shown in column V of Table 4.1, and their contour plots concerning to DE stress parameters are in Fig. 4.21. The contour plot $w_a - w_0$ is shown in Fig. 4.23 (purple regions) together with that of no-anisotropic stress. The similarity between both cases shows that data from CMB and late time background evolution are agnostic to the presence of the DE anisotropic stress.

In Fig.4.24 we include the best-fitted values of this model and others inside the 95% contour confidence plot to obtain deviations on the PS of around 10% with respect ΛCDM.

The lesson from all these models is that they leave particular and potentially detectable features in the PS, even when the parameter space for DE EoS and anisotropic parameters are allowed by CMB and background probes. In general, we found that the anisotropic stress provokes deviations smaller than 10% with respect to the ΛCDM PS at $k \sim 0.01\,h/\text{Mpc}$ for the parameters in the range $-0.30 < g_0 < 0.32$, $0 \leq c_g^2 < 0.01$ and smaller than 5% for $-0.15 < g_0 < 0.16$, $0 \leq c_g^2 < 0.01$.

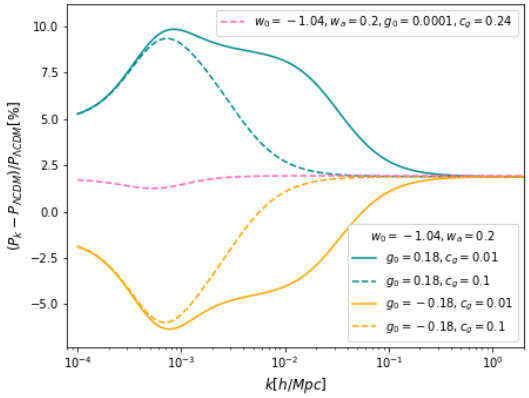

Figure 4.24: Deviations on the PS of around 10% caused by different anisotropic stress values in the 7CPL parametrization, with freezing parameters $w_0 = -1.04, w_a = 0.2$. We also include the best fitted shear parameters curve.

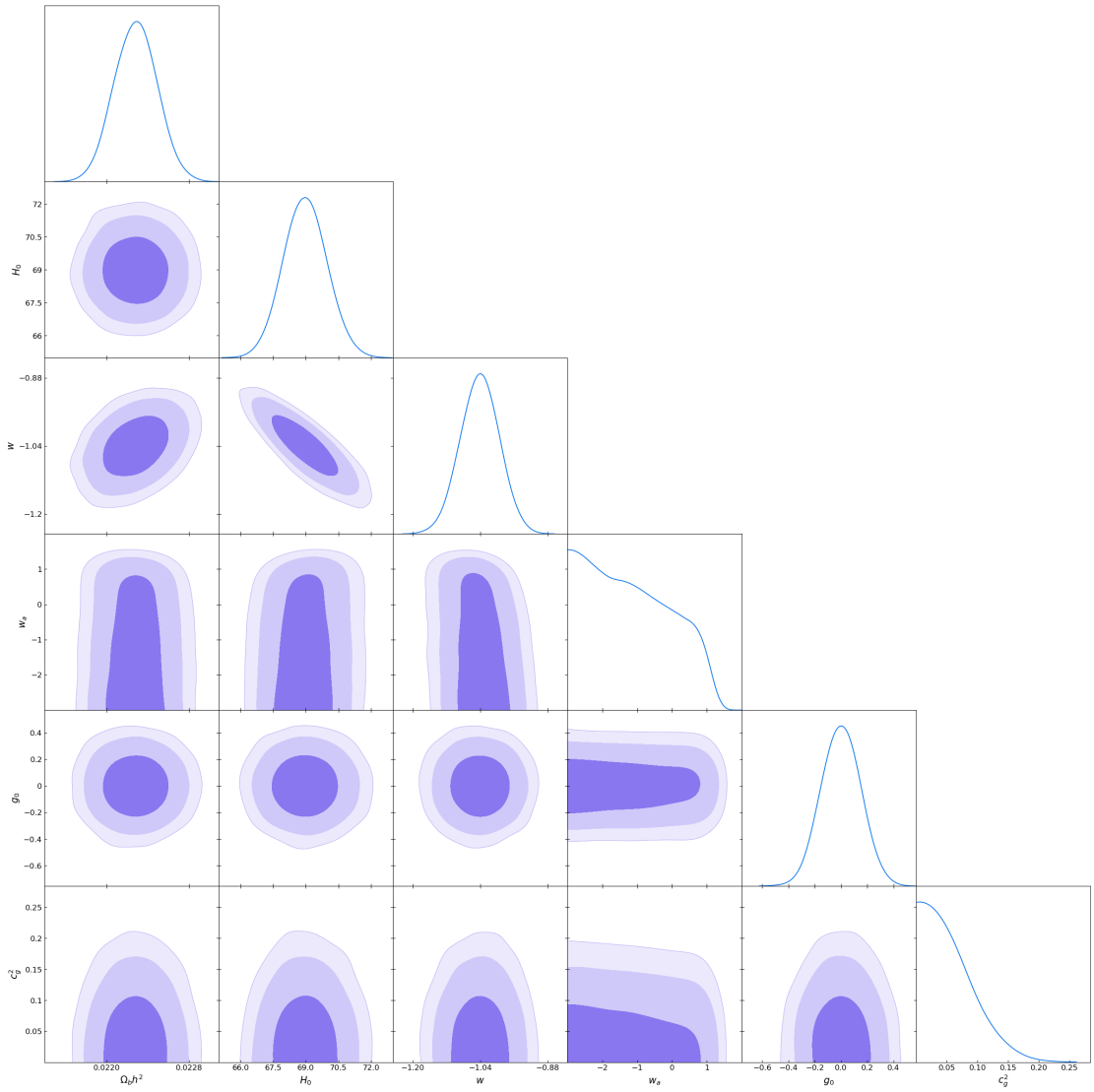

Figure 4.25: Contour confidence plots of the main cosmological parameters at 68, 95 and 99% c.l. for the 7– CPL parameterization.

Chapter 5

Conclusions

The standard cosmological model assumes general relativity as the theory of gravity, the geometry of the background is described by the FLRW metric and the matter by perfect fluids. At this level the Friedmann equations allows to establish a theoretical equation for the Hubble constant that can be measured with a variety of standard candles and rulers, all of them indicating that the universe is in an accelerated expansion epoch that is caused by an exotic matter component called dark energy in the form of a cosmological constant. Furthermore, cosmological observations for which the equations of the background are not enough can be understood in the framework of cosmological perturbation theory, this approach yields the Einstein and Navier Stokes linear equations by perturbing the FLRW background, and, allows us to confront the theoretical model with CMB anisotropies data. The standard model of cosmology is a perturbed FLRW universe whose matter content is made of radiation, baryons, cold dark matter and dark energy (as cosmological constant).

As the nature of DE is unknown it is possible to explore modifications of ΛCDM promoting the cosmological constant as a fluid with time varying EoS and adding also an anisotropic stress. The addition of the properties is easy to implement at background level, where the only modification is made through the DE density and pressure equations. However the study of perturbations can be difficult since in the equations it is introduced a divergence at $w_0 = -1$ that has to be avoided. To implement the DE perturbations there are different frameworks some of them equivalent to the MG scheme at linear order.

These DE and MG are degenerated at first order perturbation theory when DE is provided with anisotropic stress [19, 20, 21, 22]. In general, DE perturbations are smaller than DM ones, but still they may leave an imprint on the CMB and clustering evolution. The role of anisotropic stress is to create (in the $w = -1$ EoS model) or amplify/modify DE density perturbations; other effects were known to happen due to changes in the DE EoS or in its sound speed [14, 16, 15]. Anisotropic stress has an impact in the ISW effect [24, 23, 25, 26, 27, 28], that results similar for the various EoS studied in this work. But given the level of uncertainties due to the cosmic variance, CMB data alone will not shed light on such a component. However, current and forthcoming galaxy surveys can delimit this possibility.

We studied the influence of anisotropic stress parameters using the PPF formalism [25, 45] in which we employed an ansatz on the anisotropic stress function with two parameters, one mainly controlling the amplitude (g_0) and the other the scale dependence (c_g^2), such that for early times or small scales, $k \gg aHc_g^{-1}$, the stress vanishes. The best fitted parameters are shown in Table 4.1 for the different EoS considered in this work. All models predict that anisotropic stress parameters are consistent with ΛCDM model up to error bars. However, the possibility of nontrivial

anisotropic stress is open. Independent of the EoS parametrization, positive g_0 values make the perturbations to increase, the CMB TT low multipoles also increase, but the PS decreases with respect to the ΛCDM PS (negative g_0 values do the opposite). Further, we found that the parameters of the anisotropic stress and the EoS are not degenerated.

For the $w = -1$ model, CMB analysis allows any pair of values over the intervals $-1 \leq g_0 \leq 1$, $0.01 \leq c_g \leq 1$, but these are wide enough to produce large effects in the PS. In fact, parameters in the range $0.5 \leq |g_0| \leq 1$, $0.01 \leq c_g \leq 1$ reach differences with respect to ΛCDM of up to 30%, which are too big to be acceptable. The maximum percentage difference is driven by the g_0 value. In order for the anisotropic stress not to provoke deviations, with respect to ΛCDM, larger than 15% in the PS, the g_0 parameter has to be in the range $|g_0| \leq 0.32$ and for deviations of up 1% the parameter should be in the range $|g_0| \leq 0.022$. For the rest of the models considered in this work, wCDM, CPL, and 7CPL, the deviations are similar in the parameter ranges just mentioned. In general for all models, we found that in order for the anisotropic stress not to provoke deviations larger than 10% and 5% with respect to the ΛCDM PS at $k \sim 0.01\,h/\mathrm{Mpc}$, the parameters have to be in the range $-0.30 < g_0 < 0.32$, $0 \leq c_g^2 < 0.01$ and $-0.15 < g_0 < 0.16$, $0 \leq c_g^2 < 0.01$, respectively.

Since one expects that present and future galaxy surveys will have uncertainties in the determination of the PS of one-percentage levels, they could delimit the anisotropic stress stemming from DE, or equivalently from MG, to shed light on the nature of one of most mysterious components of the Universe.

Bibliography

[1] **Supernova Search Team** Collaboration, A. G. Riess *et al.*, "Observational evidence from supernovae for an accelerating universe and a cosmological constant," *Astron. J.* **116** (1998) 1009–1038, arXiv:astro-ph/9805201.

[2] **Supernova Cosmology Project** Collaboration, S. Perlmutter *et al.*, "Measurements of Ω and Λ from 42 high redshift supernovae," *Astrophys. J.* **517** (1999) 565–586, arXiv:astro-ph/9812133.

[3] **Planck** Collaboration, P. Ade *et al.*, "Planck 2015 results. XIII. Cosmological parameters," *Astron. Astrophys.* **594** (2016) A13, arXiv:1502.01589 [astro-ph.CO].

[4] D. Stern, R. Jimenez, L. Verde, M. Kamionkowski, and S. Stanford, "Cosmic Chronometers: Constraining the Equation of State of Dark Energy. I: H(z) Measurements," *JCAP* **02** (2010) 008, arXiv:0907.3149 [astro-ph.CO].

[5] C. Blake *et al.*, "The WiggleZ Dark Energy Survey: mapping the distance-redshift relation with baryon acoustic oscillations," *Mon. Not. Roy. Astron. Soc.* **418** (2011) 1707–1724, arXiv:1108.2635 [astro-ph.CO].

[6] **DES** Collaboration, T. Abbott *et al.*, "Dark Energy Survey year 1 results: Cosmological constraints from galaxy clustering and weak lensing," *Phys. Rev. D* **98** no. 4, (2018) 043526, arXiv:1708.01530 [astro-ph.CO].

[7] M. Ata *et al.*, "The clustering of the SDSS-IV extended Baryon Oscillation Spectroscopic Survey DR14 quasar sample: first measurement of baryon acoustic oscillations between redshift 0.8 and 2.2" *Mon. Not. R. Astron. Soc.* **473** no. 4, (2018) 4773–4794, arXiv:1705.06373 [astro-ph.CO].

[8] A. G. Riess, S. Casertano, W. Yuan, L. M. Macri, and D. Scolnic, "Large Magellanic Cloud Cepheid Standards Provide a 1% Foundation for the Determination of the Hubble Constant and Stronger Evidence for Physics beyond ΛCDM," *Astrophys. J.* **876** no. 1, (2019) 85, arXiv:1903.07603 [astro-ph.CO].

[9] L. Amendola and S. Tsujikawa, *Dark Energy: Theory and Observations*. Cambridge University Press, 1, 2015.

[10] P. Avelino, L. Beca, J. de Carvalho, C. Martins, and P. Pinto, "Alternatives to quintessence model-building," *Phys. Rev. D* **67** (2003) 023511, arXiv:astro-ph/0208528.

[11] H. Sandvik, M. Tegmark, M. Zaldarriaga, and I. Waga, "The end of unified dark matter?," *Phys. Rev. D* **69** (2004) 123524, arXiv:astro-ph/0212114.

[12] A. B. Balakin, D. Pavon, D. J. Schwarz, and W. Zimdahl, "Curvature force and dark energy," *New J. Phys.* **5** (2003) 85, arXiv:astro-ph/0302150.

[13] R. Bean and O. Dore, "Probing dark energy perturbations: The Dark energy equation of state and speed of sound as measured by WMAP," *Phys. Rev. D* **69** (2004) 083503, arXiv:astro-ph/0307100.

[14] J. Weller and A. Lewis, "Large scale cosmic microwave background anisotropies and dark energy," *Mon. Not. Roy. Astron. Soc.* **346** (2003) 987–993, arXiv:astro-ph/0307104.

[15] D. Huterer and D. L. Shafer, "Dark energy two decades after: Observables, probes, consistency tests," *Rept. Prog. Phys.* **81** no. 1, (2018) 016901, arXiv:1709.01091 [astro-ph.CO].

[16] R. de Putter, D. Huterer, and E. V. Linder, "Measuring the Speed of Dark: Detecting Dark Energy Perturbations," *Phys. Rev. D* **81** (2010) 103513, arXiv:1002.1311 [astro-ph.CO].

[17] **DESI** Collaboration, A. Aghamousa *et al.*, "The DESI Experiment Part I: Science,Targeting, and Survey Design," arXiv:1611.00036 [astro-ph.IM].

[18] W. Hu and D. J. Eisenstein, "The Structure of structure formation theories," *Phys. Rev. D* **59** (1999) 083509, arXiv:astro-ph/9809368.

[19] M. Kunz and D. Sapone, "Dark Energy versus Modified Gravity," *Phys. Rev. Lett.* **98** (2007) 121301, arXiv:astro-ph/0612452.

[20] Y.-S. Song, L. Hollenstein, G. Caldera-Cabral, and K. Koyama, "Theoretical Priors On Modified Growth Parametrisations," *JCAP* **04** (2010) 018, arXiv:1001.0969 [astro-ph.CO].

[21] R. Arjona, W. Cardona, and S. Nesseris, "Unraveling the effective fluid approach for $f(R)$ models in the subhorizon approximation," *Phys. Rev. D* **99** no. 4, (2019) 043516, arXiv:1811.02469 [astro-ph.CO].

[22] R. Arjona, W. Cardona, and S. Nesseris, "Designing Horndeski and the effective fluid approach," *Phys. Rev. D* **100** no. 6, (2019) 063526, arXiv:1904.06294 [astro-ph.CO].

[23] T. Koivisto and D. F. Mota, "Dark energy anisotropic stress and large scale structure formation," *Phys. Rev. D* **73** (2006) 083502, arXiv:astro-ph/0512135.

[24] W. Hu, "Structure formation with generalized dark matter," *Astrophys. J.* **506** (1998) 485–494, arXiv:astro-ph/9801234.

[25] W. Hu, "Parametrized Post-Friedmann Signatures of Acceleration in the CMB," *Phys. Rev. D* **77** (2008) 103524, arXiv:0801.2433 [astro-ph].

[26] K. Ichiki and T. Takahashi, "Constraints on Generalized Dark Energy from Recent Observations," *Phys. Rev. D* **75** (2007) 123002, arXiv:astro-ph/0703549.

[27] E. Calabrese, R. de Putter, D. Huterer, E. V. Linder, and A. Melchiorri, "Future CMB Constraints on Early, Cold, or Stressed Dark Energy," *Phys. Rev. D* **83** (2011) 023011, arXiv:1010.5612 [astro-ph.CO].

[28] B. Chang and L. Xu, "Confronting Dark Energy Anisotropic Stress," *Phys. Rev. D* **90** no. 2, (2014) 027301, arXiv:1401.6710 [astro-ph.CO].

[29] D. Mota, J. Kristiansen, T. Koivisto, and N. Groeneboom, "Constraining Dark Energy Anisotropic Stress," *Mon. Not. Roy. Astron. Soc.* **382** (2007) 793–800, arXiv:0708.0830 [astro-ph].

[30] L. Pogosian, A. Silvestri, K. Koyama, and G.-B. Zhao, "How to optimally parametrize deviations from General Relativity in the evolution of cosmological perturbations?," *Phys. Rev. D* **81** (2010) 104023, arXiv:1002.2382 [astro-ph.CO].

[31] D. Sapone and E. Majerotto, "Fingerprinting Dark Energy III: distinctive marks of viscosity," *Phys. Rev. D* **85** (2012) 123529, arXiv:1203.2157 [astro-ph.CO].

[32] W. Cardona, L. Hollenstein, and M. Kunz, "The traces of anisotropic dark energy in light of Planck," *JCAP* **07** (2014) 032, arXiv:1402.5993 [astro-ph.CO].

[33] B. Chang, J. Lu, and L. Xu, "Matter sourced anisotropic stress for dark energy," *Phys. Rev. D* **90** no. 10, (2014) 103528.

[34] W. Yang, S. Pan, L. Xu, and D. F. Mota, "Effects of anisotropic stress in interacting dark matter – dark energy scenarios," *Mon. Not. Roy. Astron. Soc.* **482** no. 2, (2019) 1858–1871, arXiv:1804.08455 [astro-ph.CO].

[35] G. Ballesteros, L. Hollenstein, R. K. Jain, and M. Kunz, "Nonlinear cosmological consistency relations and effective matter stresses," *JCAP* **05** (2012) 038, arXiv:1112.4837 [astro-ph.CO].

[36] I. Sawicki, I. D. Saltas, L. Amendola, and M. Kunz, "Consistent perturbations in an imperfect fluid," *JCAP* **01** (2013) 004, arXiv:1208.4855 [astro-ph.CO].

[37] A. Naruko, A. E. Romano, M. Sasaki, and S. A. Vallejo-Peña, "The effect of anisotropic stress and non-adiabatic pressure perturbations on the evolution of the comoving curvature perturbation," *Class. Quant. Grav.* **37** no. 1, (2020) 017001, arXiv:1804.05005 [gr-qc].

[38] D. Huterer, "Weak lensing, dark matter and dark energy," *Gen. Rel. Grav.* **42** (2010) 2177–2195, arXiv:1001.1758 [astro-ph.CO].

[39] T. Baker, P. G. Ferreira, C. D. Leonard, and M. Motta, "New Gravitational Scales in Cosmological Surveys," *Phys. Rev. D* **90** no. 12, (2014) 124030, arXiv:1409.8284 [astro-ph.CO].

[40] M. Motta, I. Sawicki, I. D. Saltas, L. Amendola, and M. Kunz, "Probing Dark Energy through Scale Dependence," *Phys. Rev. D* **88** no. 12, (2013) 124035, arXiv:1305.0008 [astro-ph.CO].

[41] L. Amendola, S. Fogli, A. Guarnizo, M. Kunz, and A. Vollmer, "Model-independent constraints on the cosmological anisotropic stress," *Phys. Rev. D* **89** no. 6, (2014) 063538, arXiv:1311.4765 [astro-ph.CO].

[42] A. M. Pinho, S. Casas, and L. Amendola, "Model-independent reconstruction of the linear anisotropic stress η," *JCAP* **11** (2018) 027, arXiv:1805.00027 [astro-ph.CO].

[43] R. Arjona and S. Nesseris, "Hints of dark energy anisotropic stress using Machine Learning," arXiv:2001.11420 [astro-ph.CO].

[44] W. Hu and I. Sawicki, "A Parameterized Post-Friedmann Framework for Modified Gravity," *Phys. Rev. D* **76** (2007) 104043, arXiv:0708.1190 [astro-ph].

[45] W. Fang, W. Hu, and A. Lewis, "Crossing the Phantom Divide with Parameterized Post-Friedmann Dark Energy," *Phys. Rev. D* **78** (2008) 087303, arXiv:0808.3125 [astro-ph].

[46] G. Garcia-Arroyo, J. L. Cervantes-Cota, U. Nucamendi, and A. Aviles, "Effects of dark energy anisotropic stress on the matter power spectrum," *Phys. Dark Univ.* **30** (2020) 100668, arXiv:2004.13917 [astro-ph.CO].

[47] K. Koyama, "Cosmological Tests of Modified Gravity," *Rept. Prog. Phys.* **79** no. 4, (2016) 046902, arXiv:1504.04623 [astro-ph.CO].

[48] T. Clifton, P. G. Ferreira, A. Padilla, and C. Skordis, "Modified Gravity and Cosmology," *Phys. Rept.* **513** (2012) 1–189, arXiv:1106.2476 [astro-ph.CO].

[49] A. G. Riess *et al.*, "New Parallaxes of Galactic Cepheids from Spatially Scanning the Hubble Space Telescope: Implications for the Hubble Constant," *Astrophys. J.* **855** no. 2, (2018) 136, arXiv:1801.01120 [astro-ph.SR].

[50] **SDSS** Collaboration, M. Betoule *et al.*, "Improved cosmological constraints from a joint analysis of the SDSS-II and SNLS supernova samples," *Astron. Astrophys.* **568** (2014) A22, arXiv:1401.4064 [astro-ph.CO].

[51] D. Scolnic *et al.*, "The Complete Light-curve Sample of Spectroscopically Confirmed SNe Ia from Pan-STARRS1 and Cosmological Constraints from the Combined Pantheon Sample," *Astrophys. J.* **859** no. 2, (2018) 101, arXiv:1710.00845 [astro-ph.CO].

[52] **SNLS** Collaboration, J. Guy *et al.*, "SALT2: Using distant supernovae to improve the use of Type Ia supernovae as distance indicators," *Astron. Astrophys.* **466** (2007) 11–21, arXiv:astro-ph/0701828.

[53] **SNLS** Collaboration, A. J. Conley *et al.*, "SiFTO: An Empirical Method for Fitting SNe Ia Light Curves," *Astrophys. J.* **681** (2008) 482–498, arXiv:0803.3441 [astro-ph].

[54] R. Kessler *et al.*, "SNANA: A Public Software Package for Supernova Analysis," *Publ. Astron. Soc. Pac.* **121** (2009) 1028, arXiv:0908.4280 [astro-ph.CO].

[55] C. Blake *et al.*, "The WiggleZ Dark Energy Survey: Joint measurements of the expansion and growth history at z ¡ 1," *Mon. Not. R. Astron. Soc.* **425** (2012) 405–414, arXiv:1204.3674 [astro-ph.CO].

[56] F. Beutler, C. Blake, M. Colless, D. Jones, L. Staveley-Smith, L. Campbell, Q. Parker, W. Saunders, and F. Watson, "The 6dF Galaxy Survey: Baryon Acoustic Oscillations and the Local Hubble Constant," *Mon. Not. R. Astron. Soc.* **416** (2011) 3017–3032, arXiv:1106.3366 [astro-ph.CO].

[57] A. J. Ross, L. Samushia, C. Howlett, W. J. Percival, A. Burden, and M. Manera, "The clustering of the SDSS DR7 main Galaxy sample – I. A 4 per cent distance measure at $z = 0.15$," *Mon. Not. R. Astron. Soc.* **449** no. 1, (2015) 835–847, arXiv:1409.3242 [astro-ph.CO].

[58] H. Gil-Marín *et al.*, "The clustering of galaxies in the SDSS-III Baryon Oscillation Spectroscopic Survey: BAO measurement from the LOS-dependent power spectrum of DR12 BOSS galaxies," *Mon. Not. R. Astron. Soc.* **460** no. 4, (2016) 4210–4219, arXiv:1509.06373 [astro-ph.CO].

[59] **BOSS** Collaboration, S. Alam *et al.*, "The clustering of galaxies in the completed SDSS-III Baryon Oscillation Spectroscopic Survey: cosmological analysis of the DR12 galaxy sample," *Mon. Not. R. Astron. Soc.* **470** no. 3, (2017) 2617–2652, arXiv:1607.03155 [astro-ph.CO].

[60] K. A. Malik and D. Wands, "Cosmological perturbations," *Phys. Rept.* **475** (2009) 1–51, arXiv:0809.4944 [astro-ph].

[61] S. Weinberg, *Cosmology*. 9, 2008.

[62] R. M. Wald, *General Relativity*. Chicago Univ. Pr., Chicago, USA, 1984.

[63] A. Lewis and A. Challinor, "Camb: Code for anisotropies in the microwave background," *Astrophysics Source Code Library* (02, 2011) 02026–. https://camb.info/.

[64] C.-P. Ma and E. Bertschinger, "Cosmological perturbation theory in the synchronous and conformal Newtonian gauges," *Astrophys. J.* **455** (1995) 7–25, arXiv:astro-ph/9506072.

[65] J. M. Bardeen, "Gauge Invariant Cosmological Perturbations," *Phys. Rev. D* **22** (1980) 1882–1905.

[66] H. Kodama and M. Sasaki, "Cosmological Perturbation Theory," *Prog. Theor. Phys. Suppl.* **78** (1984) 1–166.

[67] J. B. Dent, S. Dutta, and T. J. Weiler, "A new perspective on the relation between dark energy perturbations and the late-time ISW effect," *Phys. Rev. D* **79** (2009) 023502, arXiv:0806.3760 [astro-ph].

[68] H. Velten, R. E. Fazolo, R. von Marttens, and S. Gomes, "Degeneracy between nonadiabatic dark energy models and ΛCDM : Integrated Sachs-Wolfe effect and the cross correlation of CMB with galaxy clustering data," *Phys. Rev. D* **97** no. 10, (2018) 103514, arXiv:1803.10181 [astro-ph.CO].

[69] A. de la Macorra, "Dark Energy Parametrization motivated by Scalar Field Dynamics," *Class. Quant. Grav.* **33** no. 9, (2016) 095001, arXiv:1511.04439 [gr-qc].

[70] C. García-García, E. Bellini, P. G. Ferreira, D. Traykova, and M. Zumalacárregui, "Theoretical priors in scalar-tensor cosmologies: Thawing quintessence," *Phys. Rev. D* **101** no. 6, (2020) 063508, arXiv:1911.02868 [astro-ph.CO].

[71] R. Caldwell and E. V. Linder, "The Limits of quintessence," *Phys. Rev. Lett.* **95** (2005) 141301, arXiv:astro-ph/0505494.

[72] S. Sen, A. Sen, and M. Sami, "The thawing dark energy dynamics: Can we detect it?," *Phys. Lett. B* **686** (2010) 1–5, arXiv:0907.2814 [astro-ph.CO].

[73] P. A. R. Ade, N. Aghanim, M. Arnaud, M. Ashdown, J. Aumont, C. Baccigalupi, A. J. Banday, R. B. Barreiro, N. Bartolo, and et al., "Planck2015 results," *Astron. Astrophys.* **594** (Sep, 2016) A14.

[74] T. Hara, A. Suzuki, S. Saka, and T. Tanigawa, "Constraints for the thawing and freezing potentials," *PTEP* **2018** no. 1, (2018) 013E02, arXiv:1707.02576 [astro-ph.CO].

[75] G. Pantazis, S. Nesseris, and L. Perivolaropoulos, "Comparison of thawing and freezing dark energy parametrizations," *Phys. Rev. D* **93** no. 10, (2016) 103503, arXiv:1603.02164 [astro-ph.CO].

[76] M. Chevallier and D. Polarski, "Accelerating universes with scaling dark matter," *Int. J. Mod. Phys. D* **10** (2001) 213–224, arXiv:gr-qc/0009008.

[77] E. V. Linder, "Exploring the expansion history of the universe," *Phys. Rev. Lett.* **90** (2003) 091301, arXiv:astro-ph/0208512.

[78] J. L. Cervantes-Cota and G. Smoot, "Cosmology today-A brief review," *AIP Conf. Proc.* **1396** no. 1, (2011) 28–52, arXiv:1107.1789 [astro-ph.CO].

[79] A. Aviles, N. Cruz, J. Klapp, and O. Luongo, "Emerging the dark sector from thermodynamics of cosmological systems with constant pressure," *Gen. Rel. Grav.* **47** no. 5, (2015) 63, arXiv:1412.4185 [gr-qc].

[80] A. Lewis and S. Bridle, "Cosmological parameters from CMB and other data: A Monte Carlo approach," *Phys. Rev. D* **66** (2002) 103511, arXiv:astro-ph/0205436.

[81] A. Lewis, "Efficient sampling of fast and slow cosmological parameters," *Phys. Rev. D* **87** no. 10, (2013) 103529, arXiv:1304.4473 [astro-ph.CO].

[82] W. Yang, S. Pan, L. Xu, and D. F. Mota, "Effects of anisotropic stress in interacting dark matter – dark energy scenarios," *Mon. Not. Roy. Astron. Soc.* **482** no. 2, (2019) 1858–1871, arXiv:1804.08455 [astro-ph.CO].

[83] C. Bennett *et al.*, "Seven-Year Wilkinson Microwave Anisotropy Probe (WMAP) Observations: Are There Cosmic Microwave Background Anomalies?," *Astrophys. J. Suppl.* **192** (2011) 17, arXiv:1001.4758 [astro-ph.CO].

[84] "planck 2015 results: cosmological parameter tables." https://wiki.cosmos.esa.int/planck-legacy-archive/images/1/1a/Baseline_params_table_2015_limit95.pdf.